Politecnico di Torino

DIATI

Master Degree in Environmental Engineering - Climate Change

Ozone Monitoring

in Real-World Settings

Field Calibration and Indoor/Outdoor Dynamics

with Monica Devices

Student

Margherita Salviato

Student ID: s326840

Advisor

Prof.ssa Marina Clerico

Politecnico di Torino

Coadvisors

Ing. Davide Gallione

Ing. Nicole Mastromatteo

Politecnico di Torino

Academic Year 2024/2025

Degree's Date 21/11/2025

To Helen

Abstract

Stratospheric ozone is proved to be vital for life on Earth, whereas tropospheric ground-level ozone represents a serious threat to both plants and animals, including humans. Assessing its impacts requires comprehensive monitoring. Only 25 % of the Earth's surface has ground-based data; leaving large spatial gaps. Exposure, however, is not purely outdoor: ozone penetrates indoors and reacts with indoor pollutants, reshaping what people actually breathe. Capturing both outdoor burdens and indoor penetration is therefore essential. The aim of this work is to measure ozone levels in the summer period in both indoor and outdoor environments in the Turin area using Monica low-cost sensors. To carry out this analysis, Monica low-cost sensors were co-located close to a reference instrument (Serinus 10) for two weeks to perform a calibration. After the calibration period, the three Monica were deployed in different environments: an outdoor unit installed on the roof of the Safety Laboratory at the Politecnico di Torino; an indoor unit in a closed, rarely occupied laboratory with minimal ventilation; and an indoor unit in a laboratory that is continuously ventilated due to a permanently open window. Calibration used multivariate linear regression in hourly data using Monica's signal, temperature, and relative humidity. During deployment (30 July-30 September 2025) the outdoor unit exhibited typical summer diurnal cycles and frequent MDA8 exceedances: 18/63 days above 120 $\mu g/m^3$ and 33/63 above 100 $\mu g/m^3$. Indoors, ventilation dominated: the minimally ventilated room had low levels with weak coupling to the outdoors, while the continuously ventilated room showed higher I/O ratios and daytime peaks aligned with outdoors. A simple and transparent field calibration makes Monica sensors suitable for spatial-temporal mapping and indoor/outdoor studies.

Summary

SUMMARY

Figures List

List of Tables

1

Introduction

Ozone (O_3) is a molecule composed of three oxygen atoms that is naturally found in the atmosphere. It is possible to distinguish between ozone in the upper atmosphere, which provides essential protection, and ozone in the lower atmosphere, which is a poisonous pollutant. The ozone present in the stratosphere absorbs most of the ultraviolet light from the sun, thereby protecting life on the planet. However, O_3 is not naturally present in abundance in the troposphere; it is created by complex photochemical reactions between nitrogen oxides (NO_X) and volatile organic compounds (VOCs) from traffic, fuel evaporation and manufacturing operations. Elevated ground-level concentrations of ozone are harmful to human health and vegetation (Donzelli and Suarez-Varela 2024).

90 % of ozone is approximately concentrated in the stratosphere, an atmospheric layer that extends from about 10 to 50 km above the surface. There exists a fragile equilibrium between the processes that form and destroy ozone. Photolysis of molecular oxygen O_2 by ultraviolet radiation generates singlet oxygen atoms, which can subsequently reform with O_2 to form ozone. At the same time, ozone can be destroyed through reactions with compounds containing nitrogen, hydrogen, chlorine, or bromine. Some of these reactive species are natural; others are human-induced, such as chlorofluorocarbons (CFCs), which are responsible for the depletion of the ozone layer.

In the stratosphere, ozone represents an essential shield, entirely blocking UV-C

and absorbing most UV-B, while reducing some UV-A radiation. Earth's surface would be exposed to levels of radiation incompatible with life without this natural filter.

Ozone depletion and thinning of the protective stratospheric layer, also referred to as the "ozone hole", widespread use of synthetic compounds, such as chlorofluorocarbons (CFCs), represent a significant environmental risk, as they increase the amount of harmful UV radiation reaching the ground.

The effects on health are well known, ranging from acute impacts, such as sunburn, to long-term risks such as skin cancer, cataracts, and other kinds of eye damage. Stratospheric ozone represents a vital natural barrier for preserving life on our planet against the destructive potential of solar ultraviolet radiation (Müller 2012).

In the troposphere, closer to the ground, ozone is a secondary pollutant; this means that it is not emitted directly into the atmosphere, but is formed through complex photochemical reactions involving NO_X and VOCs of anthropogenic and natural origin. These precursors, when in the presence of solar radiation, give rise to one of the most powerful atmospheric oxidants. The balance between ozone creation and destruction is regulated not only by chemical production and loss, but also by ground deposition processes and exchange with the stratosphere. Formation and destruction are strongly linked to the VOC/NO_X ratio: in NO_X saturated conditions, typical of urban centers, ozone destruction prevails; whereas for NO_X limited but VOC abundant conditions, the production of photochemical ozone prevails, which can affect large areas even far from the original emission sources (Mousavinezhad et al. 2023).

Stratospheric ozone is proven to be vital for life on Earth, whereas tropospheric ground-level ozone represents a serious threat to both plants and animals, including humans (Donzelli and Suarez-Varela 2024).

Since the second part of the 20th century, surface ozone concentrations have risen by 30–70 % in the majority of the Northern Hemisphere. Reductions in precursors' emissions, thanks to strict regulations, are evident; however, concentra-

tions are still high and are projected to rise throughout the 21st century (Tarasick et al. 2019).

The reasons for monitoring tropospheric ozone are diverse. From a public health point of view, it is a respiratory irritant that increases the risk of cardiovascular and pulmonary diseases and leads to premature mortality. From a climatic perspective, ozone plays a crucial role in global radiative forcing and atmospheric heating. Environmentally, it destroys forest ecosystems and crops, alters soil fertility, and catalyzes the loss of biodiversity. According to future projections, towards the end of the century, biodiversity hotspots like the Mediterranean, equatorial Africa, India, and East Asia will be particularly vulnerable to high ozone levels, requiring continued monitoring (Agathokleous, Feng, et al. 2020).

Only 25 % of the Earth's surface has ground-based data; these few direct measurements are part of the problem. Satellite retrievals, despite being a powerful tool, contain biases and temporal uncertainties. However, measurements represent a crucial tool for assessing how ozone affects climate, human health, and agricultural production (Tarasick et al. 2019).

The aim of this thesis is to measure ozone levels during the summer period in the Turin area using low-cost sensors to verify the reliability of their measurements and to compare indoor versus outdoor concentrations. To carry out this analysis, Monica low-cost sensors were deployed in three different environments: an outdoor unit installed on the roof of the Safety Laboratory at the Politecnico di Torino; an indoor unit in a closed, rarely occupied laboratory with minimal ventilation; and an indoor unit in a laboratory that is continuously ventilated due to a permanently open window.

1.1 Legislative frameworks

The 2008 Directive 2008/50/EC on "Ambient air quality and cleaner air for Europe" states that one of the main goals of environmental laws is to enhance air quality. The Directive is in line with the proposed thematic plan of the Commis-

sion to reduce the number of deaths from air pollution by 40 % by 2020 compared to the 2000 level. In order to do this, it lays out steps to reduce pollution to levels that minimize detrimental impacts on the environment and human health, as well as to increase public awareness of pollution levels and associated risks. Specifically, the Directive establishes the limits, goals and responsibilities that Member States must fulfill within a specified timeframe, as well as the criteria for the assessment technique and the thresholds for each pollutant (PRQA). The reference indicator for health protection is the maximum daily average over 8 hours (MDA8), with a target value of 120 $\mu g/m^3$ that cannot be exceeded for more than 25 days per year over a three-year period. The reference indicator for vegetation is AOT40 (the sum of excesses over 80 $\mu g/m^3$ during daylight hours), which has a target value of 18 000 $\mu g/m^3 \cdot h$ (five-year average) and a long-term objective of 6000 $\mu g/m^3 \cdot h$. The directive establishes the information threshold (180 $\mu g/m^3$, 1 h) and the alert threshold (240 $\mu g/m^3$, 1 h), with mandatory rapid public information procedures in case of exceedances (European Parliament and Council of the European Union 2008). After a protracted two-year review process, the European Parliament passed Directive (EU) 2024/2881 in October 2024, which will replace Directive 2008/50/EC. This Directive will come into effect on January 1, 2030. Until then, the historical standard (MDA8 120 $\mu g/m^3$ with ≤ 25 exceedances/year as a three-year average) will be used in practice. However, it defines an MDA8 of 100 $\mu g/m^3$ at the 99th percentile (i.e., a maximum of three days per year) as a long-term health target and confirms AOT40 = 6000 $\mu g/m^3 \cdot h$ for vegetation (European Parliament and Council of the European Union 2024). In order to preserve public health, the new Directive is a significant step toward standardizing the findings of scientific studies concerning the health consequences of exposure to air pollution (European Parliament and Council of the European Union 2024). Regarding indoor ozone, the guidelines do not set limits; instead, users can refer to the values recommended by the WHO that are useful in both indoor and outdoor settings worldwide, covering all situations in which people spend time but do not address working conditions (World Health Organization 2021). The negative im-

pact of air pollution on human health, even at levels lower than previously thought, is clearly demonstrated by the 2021 Global Air Quality Guidelines (AQGs). The guidelines include lowering the levels of important air pollutants, some of which also contribute to climate change, to protect public health. According to AQGs, ozone (O_3) is one of the six "classical" pollutants whose levels must be restricted to protect public health (Organization 2021). For long-term (peak season) exposure, the AQG recommends an annual average (or seasonal average) concentration $\leq 60\,\mu g/m^3$, while for short-term exposure, the 8-hour average should not exceed $100\,\mu g/m^3$. These values correspond to the 99th percentile ($\approx$ 3–4 exceedance days per year) and are intended as health-based thresholds rather than legal limits (World Health Organization 2021). While WHO standards provide health-based benchmarks that can be used both indoors and outdoors, EU law regulates outdoor ozone with more stringent objectives.

2

Formation and Influencing Determinants of Tropospheric Ozone

Tropospheric ozone is a powerful oxidant that is not directly emitted into the atmosphere. It is formed through chemical reactions thanks to ozone precursors, such as nitrogen oxides (NO_X) and volatile organic compounds(VOCs), in the presence of sunlight (see Figure 2.1). These precursors can be natural or anthropogenic, both of which contribute significantly to the formation of ambient ozone (Donzelli and Suarez-Varela 2024).

The most important process underlying the formation of ozone is the photolysis of nitrogen dioxide (NO_2), followed by the stabilization of the atomic oxygen produced:

$$NO_2 + hv \longrightarrow NO + O(^3P) \tag{2.1}$$

$$O(^3P) + O_2 + M \longrightarrow O_3 + M \tag{2.2}$$

Where $O(^3P)$ represents an oxygen atom in the fundamental electronic state and M is the third molecule (usually N_2 or O_2) that removes excess energy by stabilizing ozone. This cycle, taken alone, does not lead to a net ozone accumulation, because the ozone can be quickly consumed by its reaction with nitric oxide (NO):

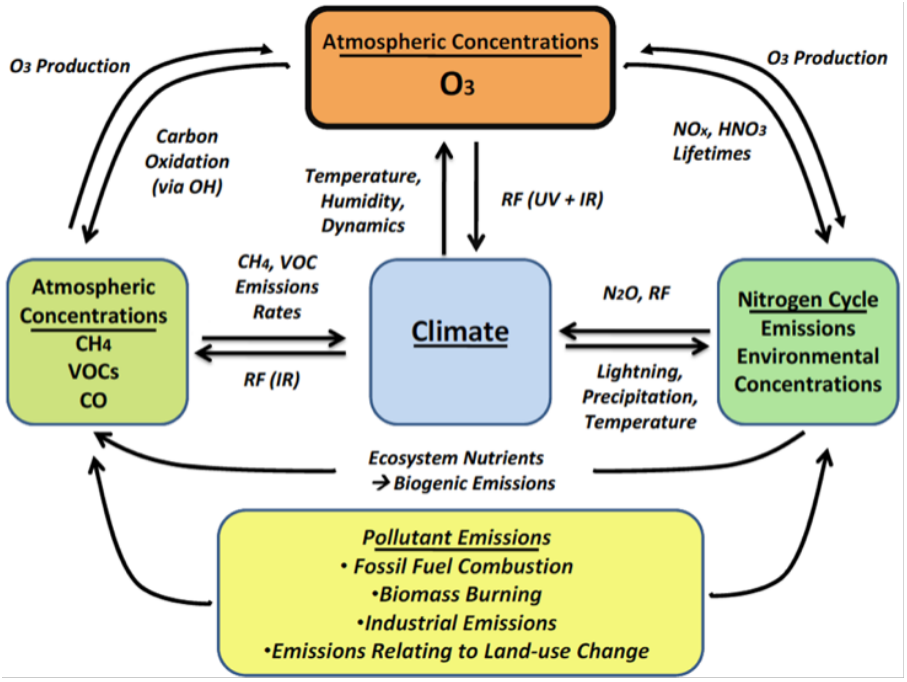

Figure 2.1: Schematic representation of the interactions of ozone in the Earth system (U.S. Environmental Protection Agency 2009)

$$O_3 + NO \longrightarrow NO_2 + O_2 \tag{2.3}$$

The continuous interconversion between NO and NO_2, mediated by reactions with ozone and solar radiation, is very quick and defines the so-called photoequilibrium of NO_X. The combination of reactions 2.1, 2.2 and 2.3 leads to the definition of the Leighton ratio (Leighton 1961), which expresses the ratio between the concentrations NO and NO_2 as a function of the ozone concentration and the kinetic parameters:

$$\frac{[NO]}{[NO_2]} = \frac{j_i}{k_{NO^+O_3}[O_3]} \tag{2.4}$$

Where j_i is the photolysis frequency of NO_2 and $k_{NO^+O_3}[O_3]$ is the bimolecular rate coefficient of the reaction NO^+O_3. This equilibrium provides a theoretical value of the expected ozone concentration, but in reality, the measured levels are often higher, confirming the fundamental role of additional radical chemistry. The prop-

agation of ozone formation is supported by OH-initiated oxidation of CO, CH_4 and VOCs. For example, carbon monoxide reacts with OH to produce peroxy radicals HO_2:

$$CO + OH + O_2 \longrightarrow CO_2 + HO_2 \tag{2.5}$$

HO_2 radicals react with NO transforming it into NO_2 without consuming ozone:

$$HO_2 + NO \longrightarrow NO_2 + OH \tag{2.6}$$

In this way, CO and VOC extend the simple (NO_X) cycle into a catalytic chain in which OH is continuously regenerated and ozone production is amplified. It is important to note that ozone itself becomes a source of OH radicals through photolysis.

$$O_3 + h\nu \longrightarrow O(^1D) + O_2 \tag{2.7}$$

$$O(^1D) + H_2O \longrightarrow 2\,OH \tag{2.8}$$

From ozone photolysis to wavelengths below 320 nm. This process regenerates OH radicals, which, in turn, oxidize new VOCs, fueling a feedback loop that leads to further ozone formation. The chemistry becomes even more complex when larger VOCs, such as alkanes, are involved. For example, for ethane (C_2H_6), the attack by OH leads to the formation of an organic peroxy radical (RO_2):

$$C_2H_6 + OH + O_2 \longrightarrow C_2H_5O_2 + H_2O \tag{2.9}$$

$$C_2H_5O_2 + NO \longrightarrow C_2H_5O + NO_2 \tag{2.10}$$

In this scheme, the organic peroxy radical (RO_2) converts NO to NO_2, thus supporting ozone production. The destiny of the resulting alkoxy radical (RO) is more complex; it can fragment, generate (HO_2) radicals, or produce new oxidized VOCs,

such as aldehydes or organic peroxides. These secondary processes further increase complexity and enrich the radical pool, strengthening the oxidative capacity of the atmosphere (Monks et al. 2015).

These mechanisms demonstrate that the photochemical generation of ozone in the troposphere is based on a fragile equilibrium among the NO_X cycle, the oxidation of VOCs, and radical propagation (Monks et al. 2015). The balance between making and breaking down ozone is not linear and depends on the ratio of VOC to NO_X. In areas with a lot of NO_X, such as city centers with heavy traffic, NO tends to react chemically with ozone, which lowers ozone levels more than expected. In contrast, in environments characterized by limited NO_X and elevated VOC levels, particularly in rural and suburban regions with significant biogenic influence, the chemical system promotes ozone production, with peak concentrations often occurring downwind as NO_X dilutes and ozone production efficiency increases (Mousavinezhad et al. 2023). The tropospheric ozone level represents a difficult air pollutant to manage because the means to lower NO_X and the VOC emissions do not always respond linearly with predictable effects. Another important aspect is that the photochemical production of ozone is part of a broader context of atmospheric chemistry; it is not an isolated phenomenon. This makes the ozone level even more difficult to predict. Ozone presence also contributes to the maintenance of the OH radical, the main oxidant of the troposphere, establishing a feedback loop that makes the system self-regenerating. Ozone represents not only a product but also a key player in regulating the oxidative capacity of the atmosphere (Sillman and He 2002).

2.1 Ozone precursors

The main chemical precursors for the formation of tropospheric ozone are nitrogen oxides (NO_X) and volatile organic compounds (VOC) (Hui et al. 2023). Most studies focus on emissions from industrial sources, forest vegetation, and urban vehicles, but it is also important to consider studies on the fundamental role of

the soil environment in contributing to NO_X and VOC emissions. A complex variety of factors influences ozone pollution, showing high spatial and temporal heterogeneity, which leads to particularly challenging control and mitigation actions (Agathokleous, De Marco, et al. 2022). In recent decades, human activities have been amplified due to the acceleration of globalization, economic development, and population growth. These kinds of human activities, such as vehicle exhaust, petrochemical combustion, and agricultural fertilization, lead to an increase in NO_X and VOCs emissions, worsening the impact on air pollution. A major source of both precursors in big cities is diesel and gasoline vehicles (Wang et al. 2017). Results indicated that over 40 % of the cities worldwide were exposed to harmful O_3 concentration ranges (40–60 $\mu g/m^3$), with most cities located in China and India (Ni et al. 2024). The formation and circulation of tropospheric ozone is also influenced by soil, because it emits and absorbs large amounts of NO_X and VOCs (Rinnan and Albers 2020).

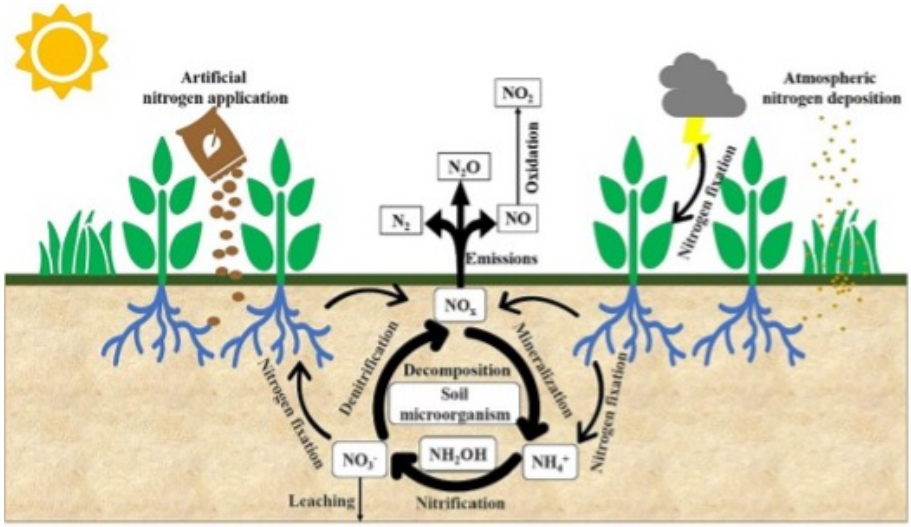

Figure 2.2: Schematic representation of Nitrogen cycle (U.S. Environmental Protection Agency 2009)

Nitrogen oxides (NO_X) are formed as by-products of nitrification and denitrification, two microbial processes that occur in many natural and agricultural ecosystems. Nitrogen oxides emitted from soils contribute 10–15 % to global NO_X emissions (Weng et al. 2020). Nitrification and denitrification by autotrophic and het-

erotrophic bacteria are key processes in the nitrogen cycle (Dewan and Lakhani 2022). Microbial processes regulate the mutually reciprocal conversion between nitrate (NO_3^-) and ammonium (NH_4^+) and release nitrogenous gasses such as NO, N_2O and N_2 into the atmosphere. The NO released into the atmosphere is converted to soil NO_X (SNO_X), a critical precursor to the formation of tropospheric ozone (Hui et al. 2023). NO_X soil emissions are usually affected by moisture, soil texture, temperature, nutrient availability, fertilizer application time and method, type of vegetation and ecosystem (Lu, Zhang, and Shen 2019, Lu, Ye, et al. 2021). In a low anthropogenic NO_X scenario, soil emissions could significantly sustain ozone production,up to 25 % of summertime NO_X (Geddes, Pusede, and Wong 2022). On hotter days, an increase in ozone production rates can be observed. SNO_X emissions account for almost half of the 2.3 ppb/°C increase in O_3 production rates, with ambient temperatures in the southeast of the United States (Romer et al. 2018). In ecosystems with large temperature variations, NO_X emissions can be influenced by temperature, mainly during periods of optimal soil moisture and high inorganic nitrogen availability. As the soil temperature increases from 30–35 °C to 35–40 °C, an average increase of 38 % of SNO_X is expected (Sha et al. 2021). SNO_X emissions are also likely to be controlled by changes in precipitation patterns and trans-evaporative fluxes (Lu, Ye, et al. 2021). It is evident that SNO_X emissions are a climate sensitive source that will contribute to high ozone scenarios. Their magnitude depends on different factors, such as temperature, soil moisture, agricultural phenology, fertilization practices, nitrogen deposition, and land management (Weng et al. 2020). It is important to note that current atmospheric models lack suitable representations of how these fluxes vary with climate change, making an evaluation of SNO_X on future ozone pollution very difficult (Lu, Ye, et al. 2021). Another major natural source of NO_X is lightning, which contributes around 10 % of the total NO_X emissions, particularly in the middle to upper troposphere, equivalent to 2–8 Tg of N per year (Kang et al. 2020). The high temperatures generated during lightning discharges lead to the dissociation of molecular oxygen into atomic oxygen (2.11), which subsequently reacts

with molecular nitrogen to form nitric oxide (NO) (2.12, 2.13) (Price, Penner, and Prather 1997).

$$O_2 \longrightarrow 2\,O \tag{2.11}$$

$$O + N_2 \longrightarrow NO + N \tag{2.12}$$

$$N + O_2 \longrightarrow NO + O \tag{2.13}$$

Lightning NO_X (LNO_X) is responsible for 35–45 % of global free tropospheric ozone production (Kang et al. 2020). The impact of lightning is strong in the middle and upper parts of the troposphere, as this region NO_X has a lifetime that is 5–10 times longer than the 1-day lifetime in the lower troposphere. LNO_X is thought to be the most important natural ozone precursor in the tropics because it is released in the middle to upper troposphere, where the lifetime of ozone is long and its production efficiency per unit NO_X is high.

VOCs are essential precursors of ozone and secondary products. In the troposphere, the dominant sources of VOCs are represented by emissions from plant leaves. VOCs are characterized by high vapor pressure and low boiling points (Dewan and Lakhani 2022).

The main Biogenic VOCs compounds are isoprene (2-methyl-1, 3-butadiene) and monoterpenes, but sesquiterpenes, alkenes, alcohols, aldehydes, and ketones are also present. These BVOCs are photooxidized and contribute significantly to the composition of the atmosphere (Weber et al. 2022). The figure 2.3 shows how BVOCs, mainly isoprene and monoterpenes, are sensitive to environmental and climate drivers. Solar radiation and temperature rise (warming) lead to an increase in emissions that enhance surface ozone levels. Drought responses are non-monotonic: mild stress can enhance emissions, while severe or prolonged drought reduces photosynthesis and BVOC emissions. Land cover change can either increase or decrease BVOCs depending on the change in vegetation. However, the net response to BVOC emissions in the future is uncertain due to the

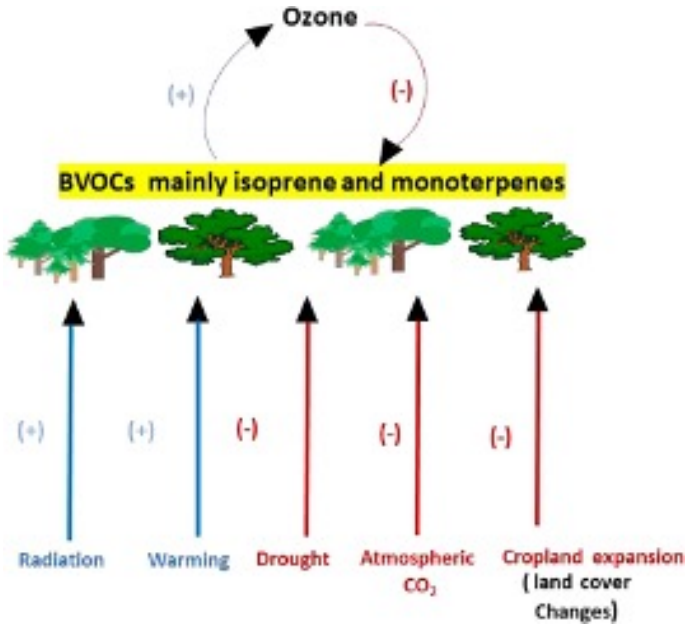

Figure 2.3: Schematic representation of the BVOCs emissions influence and ozone feedback (Dewan and Lakhani 2022)

complexity of the physical and chemical processes (Dewan and Lakhani 2022). Plant BVOC emissions are species-specific and nonlinearly influenced by temperature, sunlight, soil moisture, leaf physiology, atmospheric CO_2 mixing ratio, and other environmental factors (Trowbridge, Stoy, and Phillips 2020). Temperature changes directly affect biochemical reactions in the metabolic pathways that produce BVOCs or have indirect effects, such as lengthening the growing season (Yu et al. 2021). As temperatures increase, the enzymatic activities of synthesis are enhanced, the vapor pressure of BVOCs increases, and the resistance of the diffusion pathway is lowered. Exponential enhancements of biogenic isoprene and monoterpene emissions with increasing temperatures have been reported (Peñuelas and Staudt 2010). Isoprene can double between 20 and 30 °C (Archibald et al. 2020). However, drought and extreme heat stress reduce photosynthesis and BVOC emissions. In a study evaluating the impact of drought stress on isoprene emissions, it was calculated that, globally, biogenic isoprene emissions would be reduced by 17 % when compared to simulations that did not experience drought (Jiang et al. 2016). BVOCs emissions are difficult to estimate

due to the complexity of physical and chemical processes, mainly atmospheric CO_2, foliage composition, changes in cover in natural and managed land, and their inclusion in different models (Weber et al. 2022). BVOCs emissions will be sensitive to future climate change, land use patterns, and other environmental stressors affecting vegetation (Dewan and Lakhani 2022).

CH_4 represents both an ozone precursor and an important greenhouse gas. Its global level has risen to 1866 ppb in 2019 from 1803 ppb in 2011, mostly due to anthropogenic influences. The largest natural source of CH_4 emissions, wetlands, accounts for between 30–40 % of overall emissions and is a major concern for climate change (Gedney et al. 2019). Because methanogenesis in wet soils depends on temperature, water table depth, and organic matter, emissions are extremely sensitive to changes in climate. The 21st century is expected to see an increase in wetland CH_4 emissions. Due to a lack of knowledge regarding wetland hydrology, geochemistry, and permafrost processes, significant uncertainties persist despite their importance (Gedney et al. 2019).

2.2 Processes and feedbacks influencing tropospheric ozone

Tropospheric ozone can also be influenced by meteorology by modulating the rate of chemical kinetics, the partitioning of reaction pathways, and the efficiency of deposition. Acetaldehyde is oxidized in a hydrocarbon-rich environment with NO_X present to produce PAN.

$$CH_3CHO + OH + O_2 \longrightarrow CH_3C(O)O_2 + H_2O \tag{2.14}$$

$$CH_3C(O)O_2 + NO_2 + M \longrightarrow CH_3C(O)O_2NO_2 + M \tag{2.15}$$

In the warm lower troposphere, PAN is removed mainly via thermal decomposition; in the colder free troposphere it becomes long-lived and transportable (Talukdar

et al. 1995).

$$CH_3C(O)O_2NO_2 + M \longrightarrow CH_3C(O)O_2 + NO_2 + M \tag{2.16}$$

PAN's lifetimes depend on temperature because its decomposition rate drops significantly with decreasing temperature. This characteristic enables temperature to affect how ozone is produced and transported via PAN chemistry. PAN formation reduces ozone production close to the source region by acting as sinks for both NO_X and peroxy radicals. However, PAN can travel a great distance in the cold free troposphere, eventually thermally disintegrate to produce NO_X (usually as a result of air heating with subsidence), and hence increase ozone generation in remote areas (Fischer et al. 2014). Future temperature increases will cause PAN to undergo stronger thermal degradation, which will raise ozone in contaminated areas while lowering it in more isolated areas (Doherty et al. 2013). However, rising PAN produced by higher BVOC emissions in warmer climates can enhance PAN formation and partly offset the remote PAN decrease (Lu, Zhang, and Shen 2019).

Ozone photochemistry is also influenced by atmospheric water vapor via HO_X radical family. There are significant negative correlations between ozone concentration and relative humidity (a proxy for OH source) in remote areas with low NO_X levels because HO_X effectively removes ozone. In contrast, in polluted areas with relatively high NO_X levels, water vapor has a more complex influence. Peroxy radicals (RO_2, HO_2) are produced when OH radicals oxidize CO and hydrocarbons. The radicals facilitate the conversion of NO to NO_2 and sustain the formation of ozone. But by producing nitric acid (HNO_3), OH can also remove NO_2 from the catalytic cycle, which dampens the formation of ozone. Consequently, relationships between ozone and relative humidity in polluted air are occasionally weak, variable, or even reverse, based on measurements from a number of US and European cities. On a worldwide scale, a decrease in tropospheric ozone burden would result from rising water vapor in the warming future (Schneidemesser et al. 2015).

A 19 % increase in water vapor will lower surface mean ozone concentrations by 1–2 ppbv for the world average and 3 ppbv in the tropics (Doherty et al. 2013). Regional responses, however, can deviate from this general trend, these contrasting results highlight the competing role of water vapor in tropospheric ozone chemistry, where its net effect depends strongly on the prevailing chemical regime and the local balance between ozone production and loss pathways (Lu, Zhang, and Shen 2019).

About 20 % of the yearly total tropospheric ozone loss is attributed to dry deposition to vegetation and other surfaces, making it a significant sink of tropospheric ozone (The Royal Society 2008). The three processes of turbulent transport in the aerodynamic layer, molecular diffusion through the quasi-laminar boundary layer, and uptake at the surface are commonly used to characterize this process, which primarily takes place over vegetated surfaces via stomatal uptake on leaf surfaces and nonstomatal uptake on plant canopies (Hardacre, Wild, and Emberson 2015). The transport resistances (R_A for the aerodynamic layer, R_B for the quasi-laminar layer, and R_C for the surface) are frequently taken into account when parameterizing these mechanisms in analogy with Ohm's law (Wesely 1989). The weather, including soil moisture and air stability, has a big impact on dry deposition. Strong air stability limits dry deposition and causes a large R_A. Ozone dry deposition is usually restricted by R_C during the day when there is active turbulence activity (small R_A). R_C is further divided into nonstomatal uptake on plant canopies and the ground, as well as stomatal uptake on the leaf surface, all of which are influenced by weather. Light regulates stomata activity, which in turn affects ozone uptake through the stomata. Relative humidity and soil moisture also have an impact. Due to stomata closing to prevent transpiration, drought and high soil or air temperatures would inhibit stomatal uptake and, thus, dry deposition. This process has a major impact on ozone in semi-arid areas like the Mediterranean (Anav et al. 2018), and helps to explain the negative ozone-humidity correlations in the US (Kavassalis and Murphy 2017). Model results also showed that reductions in ozone dry deposition due to persistent high temperatures and drought could

contributed to high ozone levels in Europe (Solberg et al. 2008). Regionally, intercontinentally, and hemispherically, ozone and its precursors are transferred from their emission location to other downwind regions. Anthropogenic and biomass-burning pollution plumes have the ability to move around the world, from East Asia to North America (Monks et al. 2015). Troposphere-to-stratosphere transport (TST) and stratosphere-to-troposphere transfer (STT) make up the net stratospheric import of ozone, which is the outcome of the stratospheric-tropospheric exchange (STE). Brewer-Dobson circulation (BDC; Archibald et al. 2020) is a large-scale stratospheric meridional circulation that drives STE. In this circulation, air rises in the tropical troposphere, enters the stratosphere, is transported to the extratropical stratosphere, and then descend back into the troposphere at mid- and high latitudes. STE accounts for almost 10 % of the annual global tropospheric ozone production. One important mechanism for stratospheric intrusions (SIs) in STT episodes is the tropopause folds. Compared to their concentration in the troposphere, the air masses linked to SIs have high O_3, low CO, and low water vapor; their downward transport leads to changes in tropospheric ozone levels (Xiong et al. 2022). During folding events increases in tropospheric ozone level are observed (Akritidis et al. 2022). In addition, tropical cyclones lead to intrusion of stratospheric air into the troposphere. Ozone-rich air from the stratosphere can enter the troposphere more easily because overshooting convection linked to these systems reduces tropospheric static stability (Shen, Mickley, and Tai 2015). An increase in surface ozone levels is observed during cyclone passage, linked to the descent rate of the enhanced ozone layer. At mid latitudes over Europe, the main drivers associated with cyclones that impact surface ozone are composed of the passage of a cyclone's cold front, the ability of cyclones to bring down high levels of O_3 from the stratosphere, and associated surface high-pressure systems (Knowland et al. 2017). Weather patterns in North America and Eurasia are influenced by the El Niño-Southern Oscillation (ENSO), the Arctic Oscillation (AO), and the closely related North Atlantic Oscillation (NAO), all of which have an impact on long-range transport of ozone. It also include the Asian summer monsoon,

which provides freshwater to over a billion people. Large-scale climate variability in the coupled atmosphere-ocean system is caused by ENSO, which is the term for the interaction between the tropical Pacific's ocean and atmosphere, it influence severe weather, precipitation patterns, and agricultural productivity (Cagnazzo et al. 2009). Global atmospheric circulation, interannual fluctuations in tropospheric ozone, and precursor emissions are all impacted by ENSO, that represents a crucial climate phenomenon (Nowack et al. 2017). Tropical ozone variability is driven by ENSO-related changes in circulation, thermal patterns, and composition. Large-scale circulation anomalies associated with the Indochinese Peninsula and Indonesia produced amplified ozone plumes that extended over thousands of kilometres in the lower middle and upper troposphere (Xue et al. 2021). Another significant effect of El Niño on the tropospheric ozone column is a 20 % increase in Indonesia with the Indian Ocean region and 10 % decrease in the center region of the Pacific Ocean (Peiro et al. 2018). El Niño's warmer, drier weather promotes the burning of biomass there and may intensify lightning activity, both of which raise ozone levels (Zhang et al. 2011). Strong La Niña and El Niño events have been linked to increased tropical stratospheric water vapour (0.5 ppmv increase, approximately 70 % of the observed increase) and stratospheric moistening in the tropics (Garfinkel et al. 2018). Although positive correlations between ENSO and ozone are well established, the effects vary regionally (Hope et al. 2017).

3

Analysis of Ozone levels

To analyze ozone levels Serinus 10, an O_3 analyzer based on the principle of absorption of UV radiation was used as the reference instrument. Two units are available at the Politecnico di Torino: one located in the Safety Laboratory of the Politecnico di Torino on the roof of the fifth floor (see Figure 3.1), and another positioned in the TrAIRer (TRailer for AIR and Environmental Research), a component of the cc-moving lab mobile laboratory project. The following Table 3.1 shows the technical characteristics of the Serinus 10.

(a) Complete view (b) Close-up view

Figure 3.1: Technical cabinet with the Serinus 10 inside (UV photometric ozone analyzer, Acoem) in the Safety laboratory on Politecnico roof

Table 3.1: Technical specifications of the Serinus 10 ozone analyzer (Acoem 2023)

Serinus 10 - Ozone Analyzer	
Performance	
Range	0–20 ppm (autorange)
Concentration units	mg/m^3, $\mu g/m^3$, ng/m^3, ppm, ppb or ppt
Noise	< 0.25 ppb
Lower detectable limit	< 0.5 ppb
Linearity	< 1 % of full scale
Precision	0.5 ppb or 0.2 % of reading (whichever is greater)
Zero drift	24 hours: < 0.3 ppb; 7 days: < 0.3 ppb
Span drift	7 days: < 0.5 % of reading or < 0.3 ppb (whichever is greater)
Response time	30 s to 95 %
STP reference	0 °C, 20 °C and 25 °C at 101.3 kPa
Sample flow rate	500 cm^3/min
Temperature range	0–40 °C
Power and Dimensions	
Power supply	100–240 V_{AC}, 50–60 Hz (autorange)
Power consumption	260 VA (max at start-up), 150 VA (nominal)
Dimensions	429 mm × 175 mm × 638 mm
Rack spacing	3.5 RU
Weight	17.2 kg

To validate the Serinus 10 measurements, the data were compared with those from the Arpa Piemonte monitoring station on via Edoardo Rubino (Rubino gardens), Turin (TO), the closest station to the Polytechnic area where the O_3 data were also available (see Figure 3.2).

Arpa data related to the month of August were downloaded from the institution portal (ARPA Piemonte 2025a) and used as a regulatory reference. To ensure comparability, the time series were aligned to the same sampling interval (hourly averages) and subjected to a preliminary quality check (completeness check, removal of any manifestly incorrect or missing values). The concentrations mea-

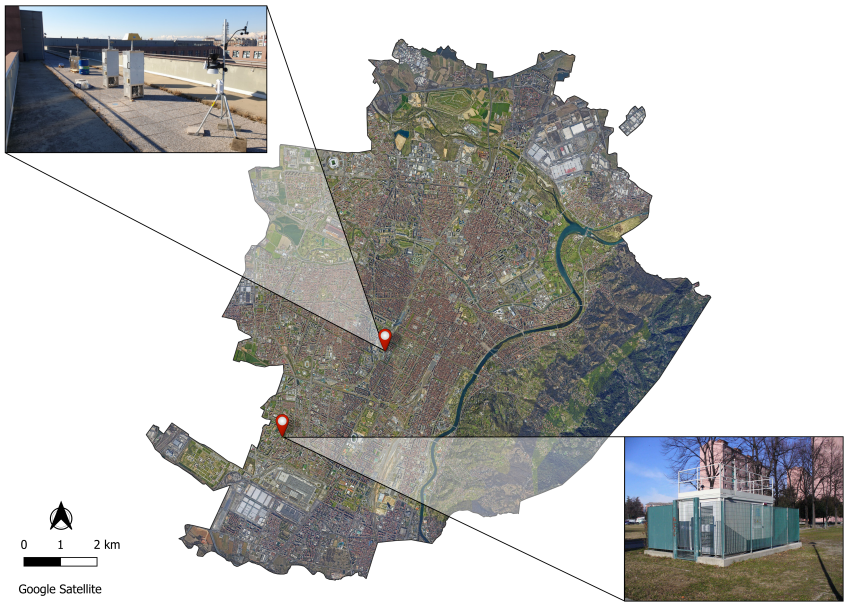

Figure 3.2: The upper marker indicates the PoliTO Safety laboratory where the Serinus 10 is located, while the lower marker shows the Arpa Piemonte Rubino reference station in Turin

sured by the Serinus 10, originally expressed in ppb, were converted to $\mu g/m^3$ according to the EPA (U.S. Environmental Protection Agency 2009) standard at 25 °C and 1 atm, applying the general relationship:

$$\mu g/m^3 = \text{ppb}\,\frac{M \cdot P}{R \cdot T}$$

where M is the molar mass of ozone (48 g/mol), P is the pressure, T is the absolute temperature and R is the constant gas. Under EPA standard conditions (298 K, 1 atm), the operating factor 1 ppb O_3 = 1.96 $\mu g/m^3$ is obtained. The conversion has been applied to the entire Serinus 10 series to allow a direct comparison with the ARPA values. Finally, a comparison was performed on synchronized series, evaluating consistency and deviations through synthetic indicators to quantify the agreement between the regulatory reference and the instrument under test.

In Figure 3.3 the comparison between the first Serinus 10, the one located on the roof and the ARPA Piemonte reference station shows excellent agreement in both temporal and statistical terms; the scatterplot indicates a correlation coeffi-

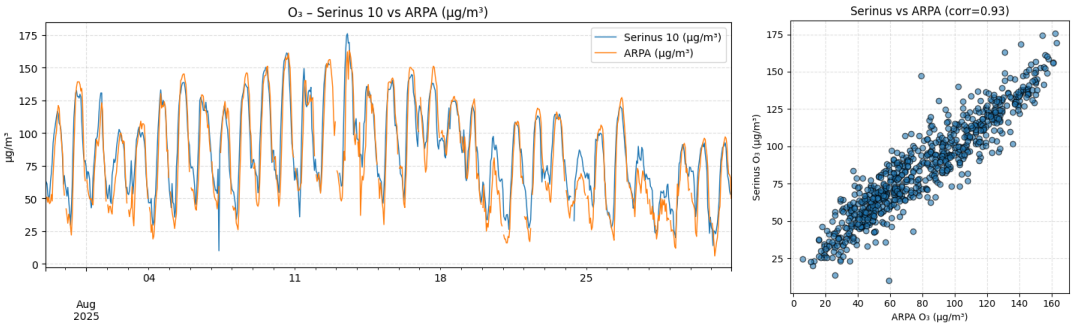

(a) Dataset 1 comparison with Serinus 10 located on the roof in PoliTO Safety laboratory

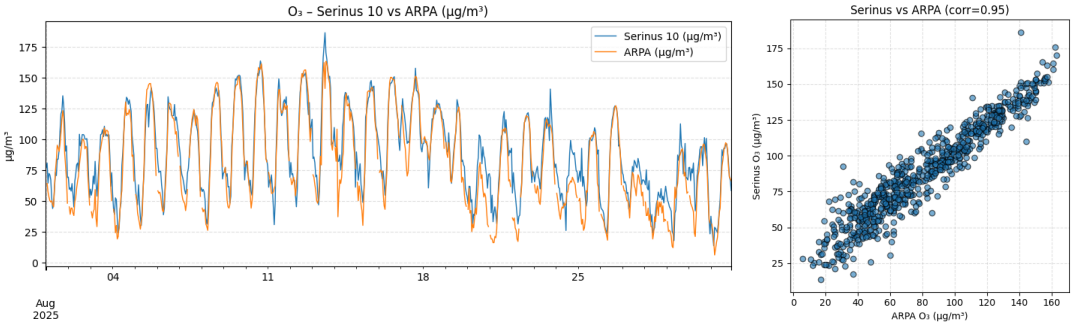

(b) Dataset 2 comparison with Serinus 10 located in the TrAIRer (cc-moving lab)

Figure 3.3: Comparison between the two Serinus 10 (one located in the Safety laboratory and the other located in the TrAIRer) and ARPA reference analyzer for ozone O_3. On the left is represented the time series and on the right there is the scatterplot

cient (R) of 0.93, while the second unit placed in the TrAIRer reaches an even higher value of 0.95, confirming a very strong linear relationship between the two datasets. Their respective time series indicate that both instruments measure identical ozone daily cycles, with a peak in the afternoon and low points at night, consistent with typical photochemical behavior. The minor differences observed are the result of a minor local variation in air mixing and position, but otherwise the magnitudes and trends of the concentrations are very uniform. Considering the high correlation coefficients, accidental time series, and physical coherence of measurement patterns, it is possible to conclude that Serinus 10 analyzers provide reliable and repeatable measurements of ambient ozone. Hence, they can be used safely as calibration and reference devices for the calibration and validation of low-cost sensors, such as the MONICA devices employed in this work.

3.1 Seasonal ozone variability

To analyze ozone levels and seasonal differences, the series recorded from October 2023 to October 2024 and from October 2024 to October 2025 are considered and displayed in Figure 3.4. As before, the Arpa series and Serinus 10 are examined. Before continuing with the analysis of these trends, it is important to point out that Serinus experienced technical problems from mid-April 2024 until mid-June 2024 and that there is also a lack of data in September 2024. Subsequently, once repaired, the data were reliable and always consistent with those indicated by Arpa; for this reason, during periods of instrument failure, the Arpa data series is taken as a reference.

The trend shown in Figure 3.4 indicates that the daily average of ozone reaches its minimum levels in December and then increases, reaching a maximum in the summer months. This behavior is consistent with what is found in the literature; in fact, the annual cycle shows that the O_3 levels are high during the warm period (May to September) and reach lower levels in November and December, with a broad ridge from May through August (Conil et al. 2025). Summer maxima (80–120 $\mu g/m^3$ between late June and August) are associated with higher temperatures and increased solar radiation, indicating a strong local photochemical component. This supports the idea that summer maxima are driven by NO_X–VOC photochemistry and a consequent decline in September/October (Jacobson 2012). Winter lows (5–20 $\mu g/m^3$ between December and January) reflect low photochemical production and efficient NO titration under more stable conditions (Jacobson 2012). The spring increase starting in March is consistent with the increase in solar radiation and the onset of photochemical activity that leads to summer maxima (Jacobson 2012). Indoor concentrations are influenced seasonally, with lower ratios in winter indirectly reflecting outdoor patterns (Nazaroff and Weschler 2022).

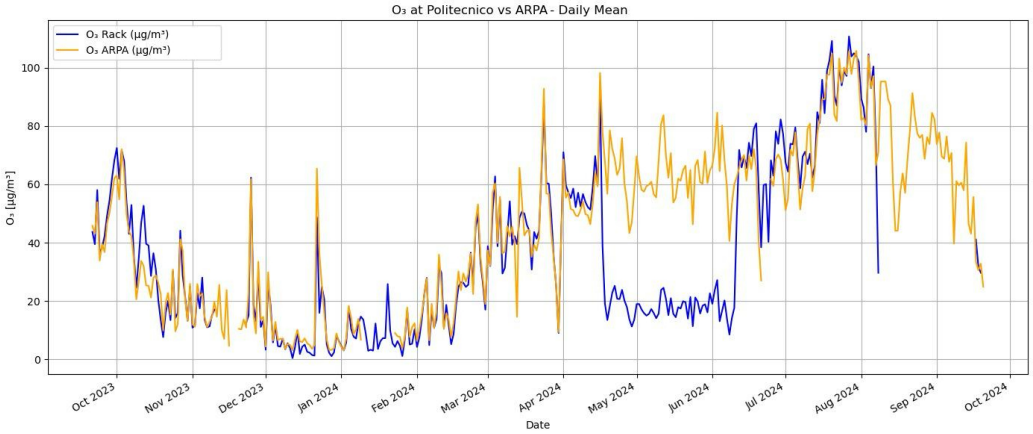

(a) Ozone series 2023-2024

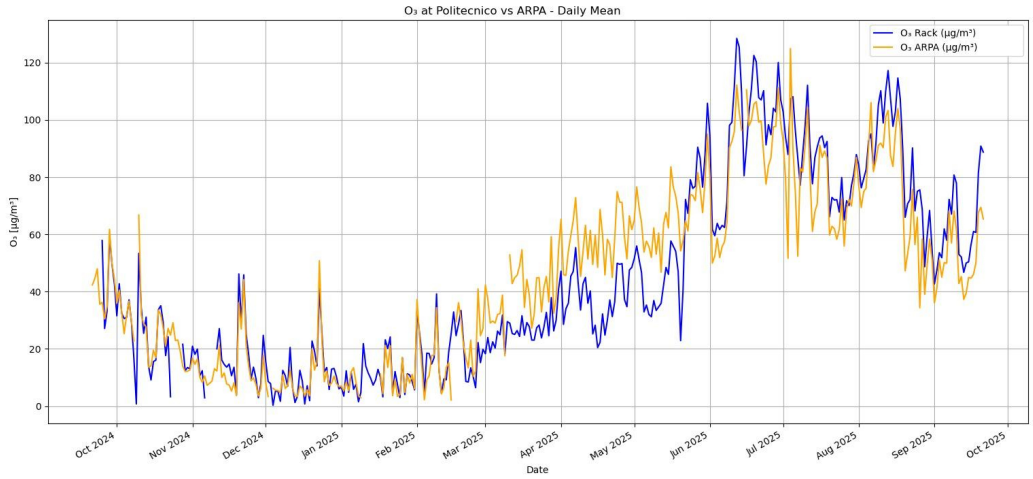

(b) Ozone series 2024-2025

Figure 3.4: Average daily concentration of O_3 at the Politecnico di Torino (Rack) and ARPA Rubino station

4

Monica sensors: Field calibration

In recent years, air quality monitoring has been transformed by low-cost air sensors designed to measure ambient particulate matter and trace gasses. While low-cost sensors may collect high-resolution temporal and geographical data on air quality, their data quality problems are typically deeper than those of conventional monitoring instruments. To overcome the problems associated with the data quality of low-cost sensors, different calibration methods have been developed. The results show that an effective technique to decrease the error is field calibration with supervised learning (Cui et al. 2021). The Monica (MONItoraggio Cooperativo della qualità dell'Aria, an acronym that translates to "Cooperative Air Quality Monitoring") system, one of the recently developed low-cost air sensors, represents a comprehensive (fixed, mobile regulatory) and participative air quality monitoring network (AQMN). The Monica architecture is based on a hybrid network that includes inexpensive portable devices that rely on arrays of electrochemical sensors and calibrated particle counters (De Vito, Esposito, et al. 2021). Monica's main aim is to make air quality assessments possible through several cooperative devices, either mobile or fixed, distributed in a specific geographic area. This system requires three domains of development. The first domain concerns the sensing nodes, which are hardware devices that measure pollutant gasses and send data. The network responsible for collecting data transmitted by the nodes and the backend that converts unprocessed data into user-friendly information is

handled by the second development domain. Presenting the results in a way that is easily understood is the third development domain (De Vito, Esposito, et al. 2021).

(a) Monica case (b) Monica inside

Figure 4.1: Monica case and the inside

The Monica device is enclosed in a robust and waterproof case (see Figure 4.1) that guaranties the protection of the electronic components against rainwater and external agents while allowing for the necessary internal ventilation. As electricity is supplied via a 230 V cable, data transmission is controlled wirelessly through an integrated 4G router or Wi-Fi connection. Inside the control unit, there is a stack of Alphasense electrochemical sensors (A4F for CO, A43F for NO_2, A431 for O_3), a Plantower optical sensor PMS7003 for particulate matter (PM_1,$PM_{2.5}$, PM_{10}) and a DHT22 sensor for temperature and relative humidity. Data is transmitted via a network connection to a cloud platform, which enables real-time display and download via the REST API, while signal gathering and processing are managed by a specialized electrical board. The general technical data are indicated in Table 4.1.

Table 4.1: Monica general technical data

GENERAL TECHNICAL DATA	
Power supply voltage	230 V_{AC}, 50–60 Hz
Maximum absorbed power	138 VA
Protection fuse F	10.3 mm × 38 mm, 1 A, 250 V_{AC}
Operating temperature	-5–40 °C
Transport and storage temperature	-10–80 °C
Operating relative humidity	10–80 % (non-condensing)
Height × Width × Depth	350 mm × 270 mm × 160 mm
Protection degree	IP23
Enclosure	Halogen-free ABS
Color	RAL7035 Grey

Tropospheric ozone monitoring in Monica is carried out using the Alphasense O_X-A431 electrochemical sensor, in combination with a dedicated NO_2-A43F sensor. The O_X-A431 is actually an oxidizing gas sensor that reacts to both ozone and nitrogen dioxide; the O_3 concentration is then determined by subtracting the correct signal of the NO_2-A43F from the O_X-A431, following adjustments for electronic offset, sensor zero, thermal dependency, and sensitivity calibration (Spinelle, Gerboles, Kok, et al. 2015). According to Monica's manual (Solerzia S.r.l. 2025), O_3-A431 has an operating range of 0–500 ppb and a data collection frequency of around 10 seconds. The values of the auxiliary electrodes (O_3Ae) and the working electrodes (O_3We), which are necessary for thermal corrections and the computation of the net signal, are supplied via the API. The following Table 4.2 shows the technical specification for the Alphasense O_X-A431 electrochemical sensor.
Monica can provide high-resolution spatial and temporal measurements at a fraction of the cost of reference stations thanks to its modular architecture and wireless connectivity. However, being a low-cost sensor leads to some advantages but also disadvantages such as the ones linked to raw signals that can be subjected to environmental interference and cross-sensitivities. For this reason, in order to significantly reduce bias and improve agreement with reference analyz-

Table 4.2: Technical specifications of the O_3 sensor Mod.A431

O_3 **- Sensor Mod.A431 (Range:** 0–500 ppb**)**	
Performance	
Sensitivity	nA/ppm at 1 ppm O_3: −650–−200 nA/ppm
Response time	t_{90} (10 ppb O_3 to 1 ppm O_3): < 60 s
Zero current	nA in zero air at 20 °C: < ±70 nA
Noise	±2 standard deviations (ppb equivalent): ±15 ppb
Range	O_3 limit of performance warranty: 20 ppm
Linearity	Error at full scale, linear at zero and 20 ppm O_3: < ±0.5 %
Cross limit	Maximum ppm for stable response to gas pulse: < 0.5 ppm
Lifetime	
Zero drift	ppb equivalent change/year in lab air: 0–20 ppb per year
Sensitivity drift	% per year in lab air (monthly test): −40–−20 % per year
Operating life	Months until 50 % original signal (24-month warranted): > 24 month

ers, field calibration campaigns combined with supervised learning models must be applied to Monica data. Field calibration was carried out on the roof of the Politecnico di Torino Safety Laboratory, three Monica devices (IDs PoliTO1, PoliTO6 and PoliTO7) were co-located on the roof as represented in Figure 4.2.

The devices were located side by side near the reference analyzer Serinus 10 at the same height. A two week calibration window was considered, starting from the 9th of July to the 23rd of July 2025, in line with Lewis and Edwards 2016 recommendations that multi-week co-location (from two to three weeks) provides sufficient variability for robust model fitting and short-term transferability. In these two weeks of calibration, it is essential to check the consistency between the three Monica, if all three behaved coherently throughout the campaign. The results are shown in the Figure 4.3.

The results of Figure 4.3 demonstrate excellent intersensor consistency during the calibration period. In panel A, daily trends are consistent with the fluctuations in ozone concentrations typical of summer dynamics. There is a slight divergence

Figure 4.2: Co-location of Monica devices on the roof in the Safety Laboratory of Politecnico di Torino

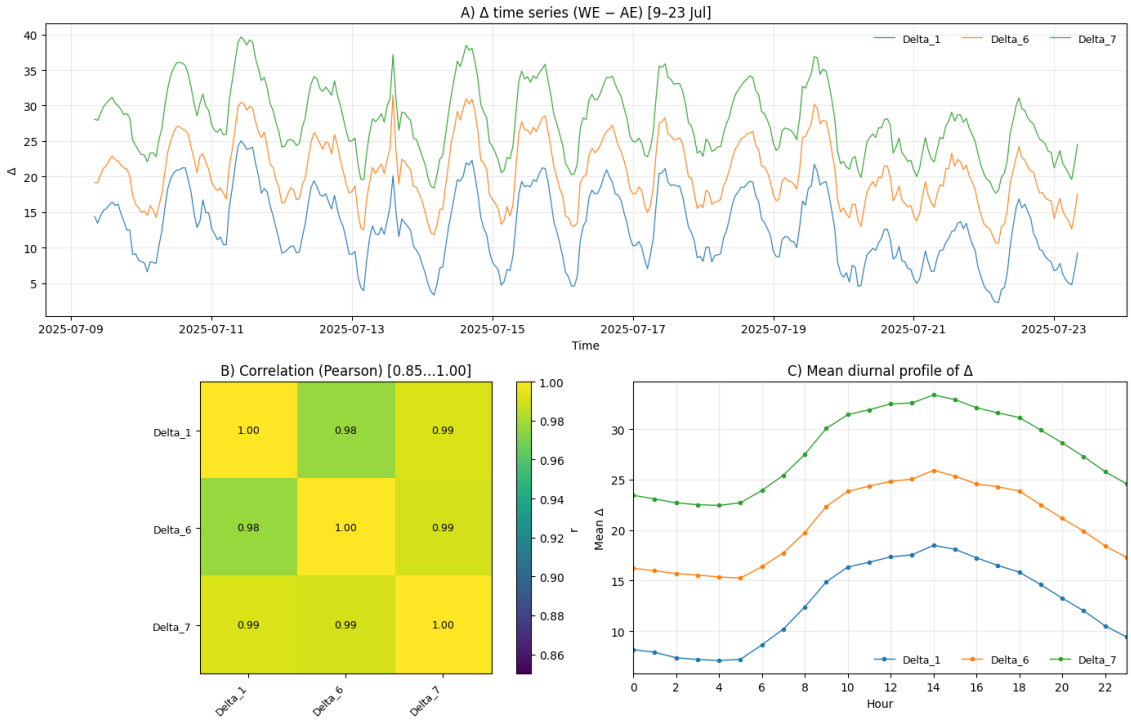

Figure 4.3: Correlation between three Monica devices during the calibration period

in the sensitivity response of the individual sensors, probably due to different internal conditions, which can be compensated for during the calibration procedure

with reference to the Serinus 10. The Pearson correlation in Panel B shows very high values, ranging from 0.98 to 0.99, confirming the temporal consistency and stability between the sensors. The average daytime profile of delta in the C panel reveals a smooth and consistent pattern among the 3 devices. These features support the quality of the data collected and the validity of the calibration interval chosen for model training. In order to proceed with calibration, the Monica signal (Δ = WE – AE) is taken into account, where WE represents the working electrode and AE is an auxiliary electrode that measures the impact of drift and background noise. The Serinus 10 UV photometric O_3 analyzer, compliant with EN 14625 and previously presented in the preceding chapter, is used as a reference tool. Multiple linear regression (MLR) was used as a calibration model, a choice supported by the literature on low-cost sensors (Spinelle, Gerboles, Kok, et al. 2015, Lewis and Edwards 2016). This methodology combines simplicity of interpretation with the ability to include environmental variables, such as temperature and humidity, to improve correspondence with reference measurements. Three predictors were used for the definition of the MLR model: the main variable (Δ), the temperature and relative humidity, which, according to the study by Spinelle, Gerboles, Kok, et al. 2015, are the main causes of nonlinearity and hysteresis in the ozone detection sensors used by Monica. The same study shows that the inclusion of weather variables (in appendix A temperature, relative humidity, radiation and daily rainfall are represented) improves performance compared to a simple univariate regression. In Figure (4.4) below are the results of the calibration of the 3 devices.
A fundamental step is time synchronization; then the aggregated hourly averages were calculated, and outliers were removed. Then, multiple linear regression was used to estimate the hourly concentration of ozone from the electrochemical differentials and environmental variables. The operating specification is as follows:

$$O_3(t) = \beta_0 + \beta_1, \Delta O_3(t) + \beta_2, T_t + \beta_3, RH_t \tag{4.1}$$

where T is the air temperature and RH is the relative humidity. As presented in

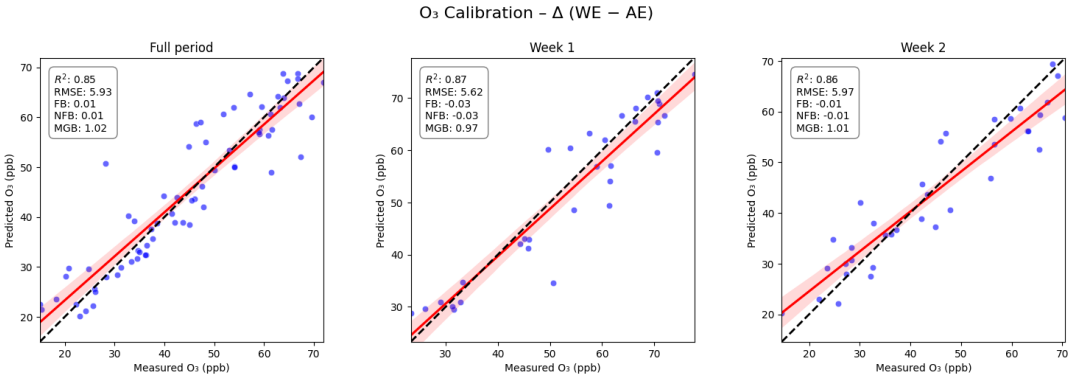

(a) PoliTO1

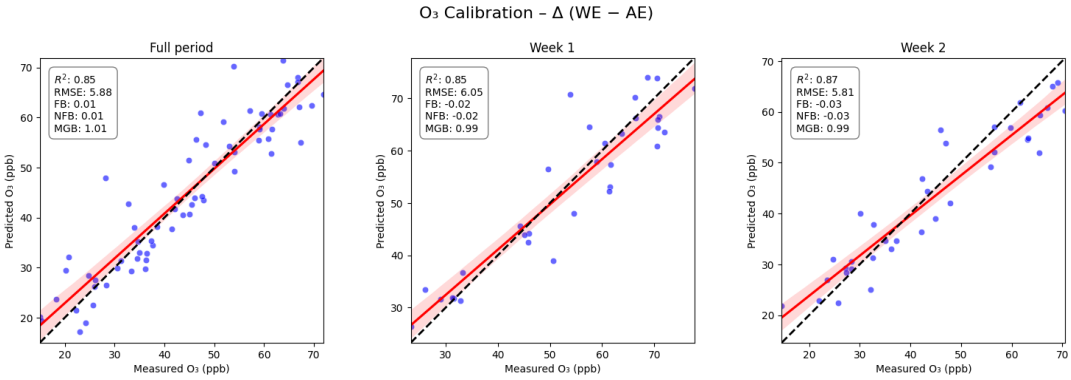

(b) PoliTO6

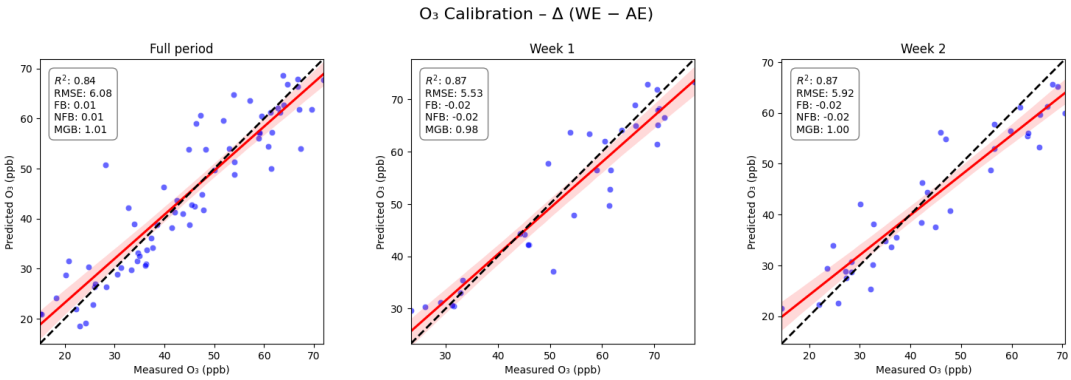

(c) PoliTO7

Figure 4.4: Calibration plots of the three Monica devices located at the Politecnico di Torino site

Figure 4.4, all the devices show a good linear correlation with the Serinus 10. This is confirmed by the R^2 values, which range from 0.84 to 0.87 for the entire calibration period. The root mean square error (RMSE) is around 5.8–6 ppb, consistent with the existing literature for the calibration of low cost sensors (Spinelle, Ger-

boles, Villani, et al. 2017, De Vito, Del Giudice, et al. 2023). For all three devices, the fractional bias (FB) and normalized fractional bias (NFB) are close to zero and the mean gain bias (MGB) is close to one. These indicators confirm the absence of systematic bias, verify the correct response scale, and indicate that the calibration is well balanced and stable over time. To assess the dataset's stability, it is useful to compare the first and second weeks of calibration. There is no visible drift during the calibration phase, as evidenced by the nearly equal performance between the first and second weeks of the data. With less dispersion at both low and high O_3 concentrations, the regression lines (in red) consistently follow the bisector (black dotted line). To verify calibration, Figure 4.5 shows the trends of the calibrated O_3 series compared to reference O_3 (Serinus 10), along with relative scatter plots to verify their linearity and agreement. Performance is stable; R^2 values are between 0.853 and 0.861, with RMSE values between 5.76 and 5.95 ppb. These values are consistent with the literature on low-cost sensors and are satisfactory for further analysis (Spinelle, Gerboles, Kok, et al. 2015). A slight underestimation of the peaks and an overestimation of the lows are observed, an effect that will be considered in the interpretation of the results.

The calibration procedure follows the 2008/50/EC Directive, which defines the assessment criteria, reference methods, and operational thresholds for tropospheric ozone. This framework has been updated by Directive (EU) 2024/2881; therefore the calibration procedure is carried out in line with the updated assessment requirements and the more stringent ozone limits, which move closer to the WHO 2021 Air Quality Guidelines. The reference instrument for calibration is the Serinus 10, an EN 14625 compliant analyzer (UV photometry); this ensures that the measurements derive from methods officially recognized as a regulatory reference. The three devices, PoliTO1, PoliTO6, and PoliTO7, were installed in an urban site with free air circulation, according to the location criteria of Annex IV. The measurements are consistent with the data quality objectives, which ensure that, prior to analysis, the data have been verified and cleaned to obtain a representative dataset suitable for multivariate regression. Monica-Serinus 10 data used in

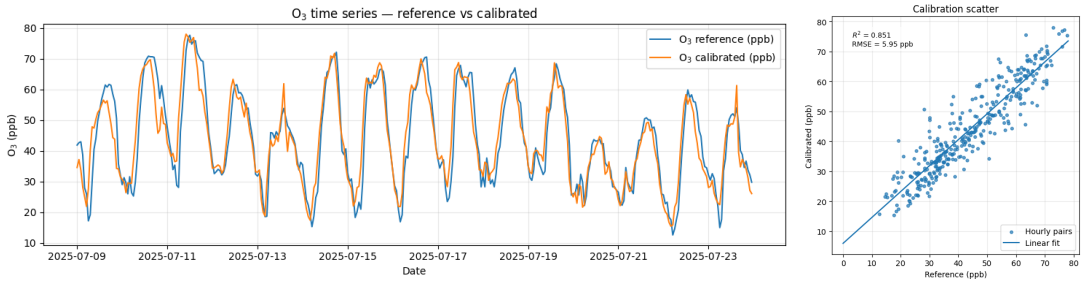

(a) PoliTO1 series

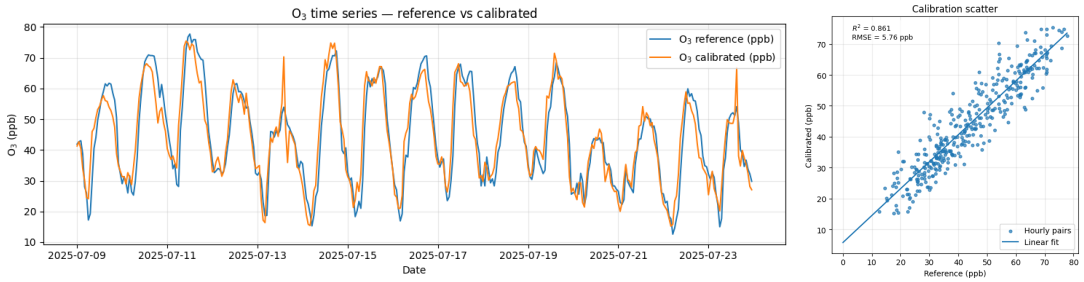

(b) PoliTO6 series

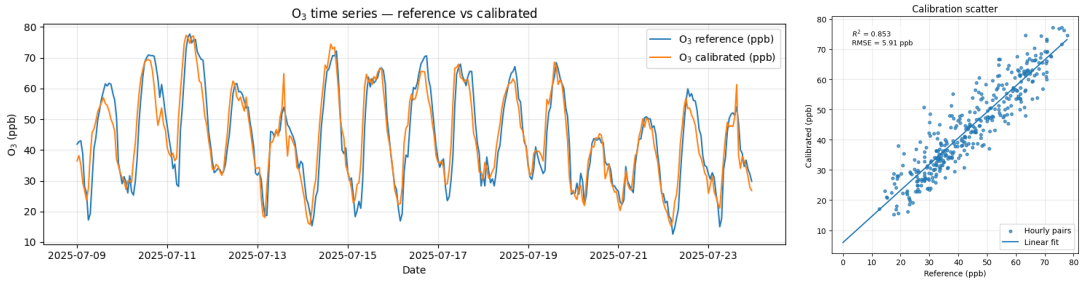

(c) PoliTO7 series

Figure 4.5: Comparison between the Serinus 10 and calibrated O_3, with the instruments co-located at the same site during the calibration period (9 - 23 July). On the left is represented the timeseries and on the right the scatterplot

the analyzes comply with the operational provisions of Directive (EU) 2024/2881 for the assessment of ozone because they follow the quality requirements of the absence of systematic bias and week-to-week stability.

4.1 Calibration stability

Directive (EU) 2024/2881, which replaces Directive 2008/50/EC, explicitly introduces verification requirements, periodic checks are recommended for sensors

prone to drift (European Parliament and Council of the European Union 2024). Although the new Directive does not specify the exact frequency of these checks (European Parliament and Council of the European Union 2024); evidence from field campaigns shows that sensor predictions can drift over multimonth deployments (Spinelle, Gerboles, Kok, et al. 2015). Therefore, given the possibility of verification due to the co-location of the Serinus reference instrument and the PoliTO6 device, verification was carried out for the August and September calibrations in accordance with the general requirement to confirm laboratory-derived models during field exposure. The Serinus 10 values were compared with those of Monica, with ID PoliTO6, since both are located in the Safety Laboratory on the roof of the Politecnico di Torino. The results shown in Figure 4.6 indicate that the calibration for the month of August remains stable, showing negligible deviations from the two weeks in July used for the initial calibration. In September, consistency was also excellent, with only minimal differences compared to August.

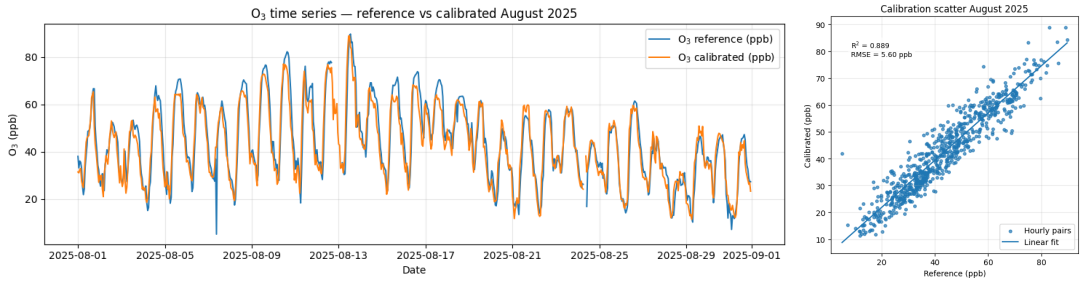

(a) August

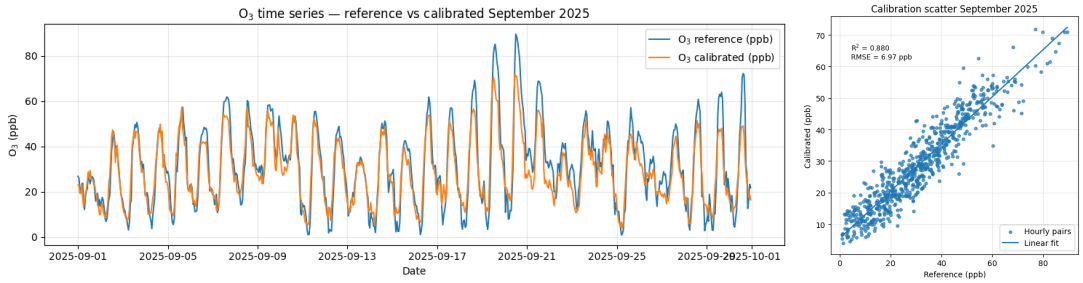

(b) September

Figure 4.6: Comparison between the Serinus 10 and the calibrated PoliTO6 O_3 measurements for August and September, with the instruments co-located at the same site. On the left is represented the timeseries and on the right the scatterplot

5

Measurement campaign

After conducting the calibration campaign for the measurement of tropospheric ozone with low-cost sensors, the data measurements were conducted in three representative microenvironments.

(a) Monica PoliTO1 placement (b) Monica PoliTO1 laboratory

Figure 5.1: PoliTO1 placement in laboratory

The Monica with PoliTO1 ID was kept in a confined, rarely used Polytechnic laboratory with a south-east orientation, as shown in Figure 5.1. The room is not

mechanically ventilated and is rarely opened. It is possible to assess the sensor's reaction in the absence of mechanical turbulence under constant thermal settings. In these contexts, attenuated O_3 variability due to surface deposition and reduced photolysis is expected, factors that help to test the stability of the model in a quasi-stationary state.

Figure 5.2: PoliTO6 placement on the roof

The Monica with PoliTO6 ID was left on the roof in the Safety laboratory, as shown in Figure 5.2, near the Serinus 10, to monitor an outdoor environment exposed to rapid changes in temperature, humidity, and radiation under real conditions. The proximity to the calibration reference instrument, the Serinus 10, allowed for cross-checking of calibration consistency under real-world conditions, as recommended for post-calibration consistency checks (Spinelle, Gerboles, Kok, et al. 2015).
The PoliTO7 Monica was placed in a west oriented Politecnico laboratory with continuous natural ventilation, as seen in the Figure 5.3. A window was kept open throughout the data collection process, ensuring a steady flow of air and minimizing the effects of stagnation. This setting is perfect for evaluating the temporal stability of the MLR model when modest weather fluctuations are present. The

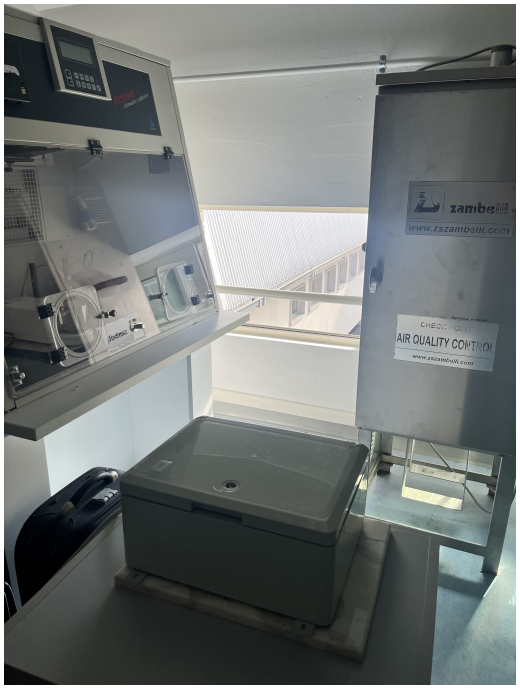

(a) Monica PoliTO7 placement

(b) Open window throughout the data gathering process

Figure 5.3: PoliTO7 placement in laboratory

multienvironment technique makes it possible to confirm that the calibration parameters are robust both indoors, where there is less interference from VOCs and NO_X and outdoors, where drift effects and interference are more noticeable. Following Monica's installation in the three previously mentioned environments, two months of continuous data collection were initiated, specifically from July 30 to September 30. Temperature, humidity, O_3We, and O_3Ae data were collected for each Monica, synchronized on the same time axis, and sampled as hourly averages. Regarding calibration, temporal coverage was checked, any discontinuities were documented, and any missing values were removed from the final dataset. Temperature and humidity were used as microclimatic correctors, and the differential $\Delta = O_3We - O_3Ae$ was calculated from the electrochemical signal as the primary variable.

5.1 Results

The findings presented are derived from the measurement campaign conducted between 30 July and 30 September 2025, a weekly and monthly representation is shown in appendix B. To ensure a more comprehensive overview, the analysis began with the outdoor data, followed by the indoor data, with comments provided on the daily profiles for the three different environments just described (PoliTO1, PoliTO6 and PoliTO7). For the PoliTO6 Monica unit, the reported values are outdoor ozone concentrations; therefore, they require different considerations than indoor cases. In central and western Europe, ozone levels show a very marked seasonal cycle. The intraseasonal variability of surface ozone anomalies revealed two distinct periods: a cold period from November to February and a warmer period from April to September (Conil et al. 2025). The monitoring period of this case study falls within the latter. The annual cycle shows that O_3 levels are high during the warm period (May-September). This was also confirmed in Boleti et al. (2020), where a group of Western European stations exhibits a seasonal cycle with minima in November-December and a broad ridge from May through August. The summer daytime profile is articulated with a maximum in the early afternoon ($90\,\mu g/m^3$) and a minimum at night, reflecting active photoproduction and a deeper boundary layer during the hot hours (Conil et al. 2025). In an urban setting, the ozone trend exhibits typical summer behavior. The graph in Figure 5.4 displays significant fluctuations in daylight, with high and frequent levels in August and a sudden decrease in September. Table 5.1 displays the mean and median values for the entire period, as well as the variation between August and September. The average is $81.8\,\mu g/m^3$ in August and $56.8\,\mu g/m^3$ in September, consistent with the seasonal plateau in late spring and summer, and the early autumn decline reported in long-term records (Conil et al. 2025). August's peaks have higher amplitudes, which is consistent with warmer, drier, and more irradiated days that increase photochemical production (Conil et al. 2025). September exhibited a gradual decrease that aligned with a reduction in solar radiation and

photochemical production, as well as a windier and more variable weather (Boleti et al. 2020).

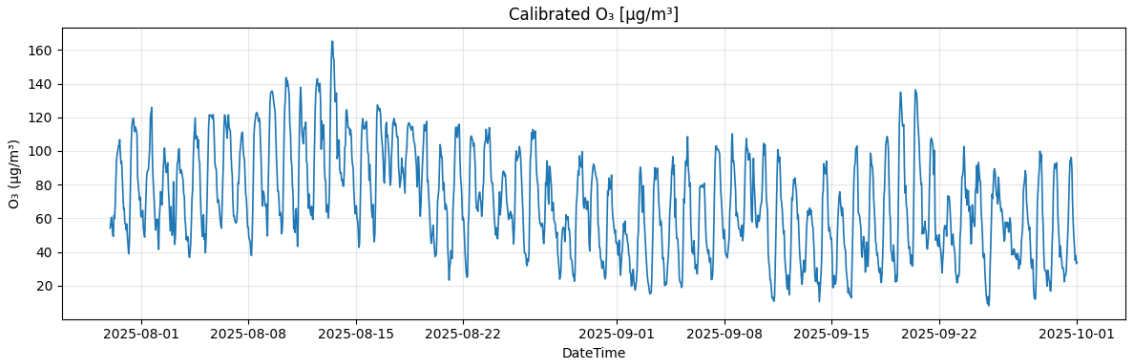

Figure 5.4: Time series of calibrated outdoor O_3 ($\mu g/m^3$) measured by the Monica sensor (PoliTO6) July 30-September 30

Table 5.1: Outdoor ozone: hourly mean and median concentrations for PoliTO6

Period	**Mean** ($\mu g/m^3$)	**Median** ($\mu g/m^3$)
30 Jul-30 Sep	69.7	67.2
August 2025	81.8	83.0
September 2025	56.8	59.2

Before moving on to the results for indoor environments, it is necessary to define the I/O ratio, which is the ratio between the average ozone concentration measured within a building and the average ozone concentration recorded outside (Nazaroff and Weschler 2022). In reality, it represents the percentage of ozone from the surrounding air that is still present in the constructed environment after penetration, ventilation, and removal procedures. This ratio corresponds to the infiltration factor (FO_3), or the interior concentration adjusted to the outdoor one, in the absence of internal sources of ozone. The value of FO_3 depends on three sets of physicochemical factors:

(i) the entry of air from outside, summarized by the exchange rate (λ) and the penetration factor (P) along the infiltration or ventilation paths;

(ii) first-order indoor losses summarized in (K) (sum of deposition on surfaces, reactions on occupants and materials, titration with NO);

(iii) configuration of the use of the building (openings, opening hours, occupancy) (Nazaroff and Weschler 2022).

The average concentrations of indoor ozone are typically between 4 and 6 ppb, with an indoor-to-outdoor concentration ratio of approximately 25 %. Considerable variability exists in this ratio between buildings, as influenced by seven building-associated factors: ozone removal in mechanical ventilation systems, ozone penetration through the building envelope, air-change rates, ozone loss rates on fixed indoor surfaces, ozone loss rates on human occupants, ozone loss by homogeneous reaction with nitrogen oxides and ozone loss by reaction with gas-phase organics. Indoor emission sources can significantly increase indoor ozone concentrations, although most indoor ozone comes from outside and enters through ventilation air (World Health Organization 2006). More than 2000 indoor environments were examined in the Nazaroff and Weschler (2022) study, and the I/O ratio is often higher during summer (high ozone season) in addition to elevated indoor ozone concentrations compared to other seasons. Upland, California, research provides a notable example, with an I/O ratio of 24 % during the high ozone season (11.8 ppb indoors vs. 48.2 ppb outdoors) and only 15 % during the milder months (3.2 ppb indoors vs. 21.1 ppb outdoors) (Geyh, Özkaynak, and Spengler 2000). In an indoor scenario, the air exchange rate (λ) and the first-order loss on indoor surfaces ($k_d\left(\frac{A}{V}\right)$) are the main factors influencing the indoor outdoor ozone ratio (I/O). A common way to describe the relationship is this:

$$\mathrm{I/O} = \frac{\lambda}{\lambda + k_d\left(\frac{A}{V}\right)} \tag{5.1}$$

where $\frac{A}{V}$ is the surface-to-volume ratio of the room (Nazaroff and Weschler 2022). For the first Monica examined, the one with PoliTO1 ID, which is shown in Figure 5.1 and previously described, only a small portion of the external ozone penetrates inside when λ is low, as the surface loss term dominates the denominator of the equation 5.1. As a result, the interior time series shows a flat baseline with occasional increases that correspond to brief window or door openings, and

ozone concentrations in a poorly ventilated space are significantly attenuated compared to outdoor values. These premises allow for the analysis of the first Monica PoliTO1 data, which is shown in graph 5.5 and displays the hourly trend of calibrated ozone in the environment under study. The results are in line with what has been reported in the literature; in fact, the signal is attenuated compared to the external environment. With episodic peaks and a flatter trend towards September. This shows that limited air exchange attenuates the entry of ozone from outside. The hourly coverage shown in Table 5.2 of valid indoor-outdoor hours enables us to assess the reliability of the I/O ratio estimations and identify any biases resulting from missing data. the high hourly coverage ensures a strong estimate of the I/O ratio and a lower risk of bias, which is 97.6 % for the entire period (30 July-30 September), with 95.2 % in August and 100 % in September. The general median of the series is 6.5 $\mu g/m^3$. The I/O value reported in the present study is 0.107, which is lower than the central tendency commonly reported in the literature (around 0.25). These values are consistent with a low air exchange regime in which surface losses dominate ventilation, resulting in a strong attenuation of outdoor ozone indoors. Both the I/O ratio and the indoor median decrease in September, indicating that the laboratory operates under a low turnover regime and that the indoor response to the seasonality of outdoor ozone is reduced.

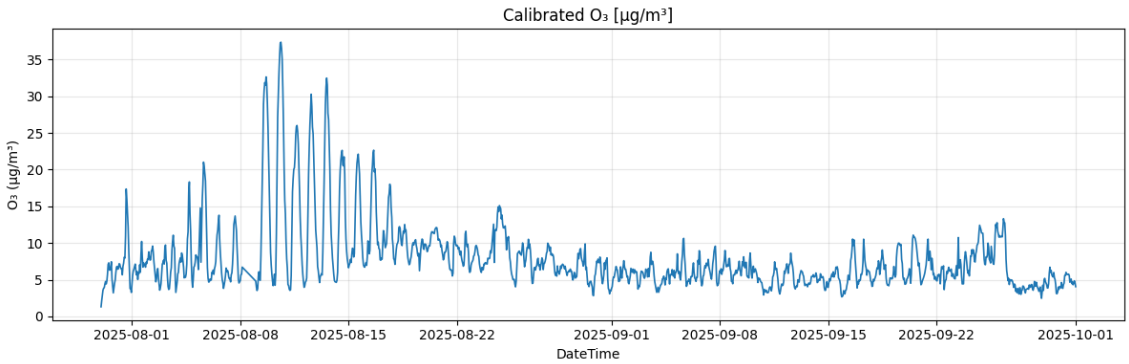

Figure 5.5: Time series of calibrated O_3 ($\mu g/m^3$) measured by the Monica sensor (PoliTO1) July 30-September 30, in an isolated, non-ventilated room

For Monica, with PoliTO7 ID, placed in an indoor environment with continuous

Table 5.2: Hourly coverage, indoor median, and I/O ratio of PoliTO1

Period	**Hourly coverage**	**Indoor median** ($\mu g/m^3$)	**I/O ratio**
30 Jul-30 Sep	97.6 %	6.5	0.107
August 2025	95.2 %	8.1	0.116
September 2025	100 %	5.6	0.097

Notes. The indoor median is the median calibrated O_3 concentration in $\mu g/m^3$. The I/O ratio is computed as the *ratio of means* (mean indoor / mean outdoor) over the same valid hourly samples.

natural ventilation, thanks to a window that is always open, the data have a very high hourly coverage valid for indoor-outdoor conditions, as indicated in the Table 5.3. This verification confirms that the I/O ratio estimates are reliable and that there are no biases due to missing data. Data in Figure 5.6 show an indoor behavior closely coupled with the outdoors, as expected under conditions of high air exchange and almost complete ozone penetration. The I/O ratio for the entire period considered (30 July-30 September) is 0.432, indicating that the internal levels replicate the external levels. This I/O ratio value is significantly higher than the PoliTO1 value, where the I/O ratio is about 0.107, reflecting the stronger ventilation regime. The measured I/O value of 0.432 for PoliTO7 is consistent with the formula 5.1, which predicts a substantial increase in the ratio when the air exchange rate λ increases. For naturally ventilated spaces literature indicates that moderate-high λ (order 1–3 per h) typically yields I/O in the 0.3–0.6 range, while very high λ (windows persistently open and strong driving forces) can push I/O toward (around 0.8) in extreme cases Nazaroff and Weschler (2022). The observed values at PoliTO7 (overall 0.43, peaking near 0.50 in August) therefore fall within the expected range for a continuously ventilated indoor environment. The previously mentioned analysis is confirmed by a month-by-month examination. In August, the I/O ratio is 0.493, and the median indoor ozone concentration is $41.5\,\mu g/m^3$. This demonstrates the correlation between the indoor and outdoor series, which suggests continuous ventilation. In September, the I/O ratio is 0.342, and the median indoor concentration is $19.1\,\mu g/m^3$. This indicates a slight decrease in the correlation, which is indicative of weaker outside forcing. Regarding indoor sec-

ondary chemistry, the specific operational conditions in this environment, such as rarely used spaces, lack of cleaning activities, and natural ventilation via a permanently open window, limit the likelihood of substantial indoor ozonolysis. Usually, in typical occupied settings, the presence of reactive organic compounds (particularly terpenes such as d-limonene and α-pinene) emitted by detergents, perfumes, or materials causes ozonolysis reactions that generate reactive intermediates and a variety of by-products, including aldehydes, organic acids, peroxides, and secondary organic particulate matter (SOA) in the ultrafine fraction (Weschler and Shields 2000). Similar processes take place on organic surfaces and films (including skin lipids such as squalene on skin and tissues), which help remove O_3 while simultaneously forming oxidized compounds that may irritate (Liu et al. 2015). Therefore, in this case, the absence of occupants and cleaning strongly reduces these precursors and surface films. the observed indoor dynamics are best explained by ventilation-driven penetration and surface deposition, rather than by in-situ chemistry. High I/O should not be exclusively seen as "good ventilation" because an increase in available O_3 may cause the production of byproducts that could irritate the respiratory tract and mucous membranes and raise the amount of ultrafine particulate matter (World Health Organization 2006). However, in this low-activity laboratory, such pathways are likely weak; if occupancy or cleaning patterns change, targeted co-pollutant measurements (e.g., carbonyls, ultrafine particle number) would be needed to reassess the role of secondary chemistry.

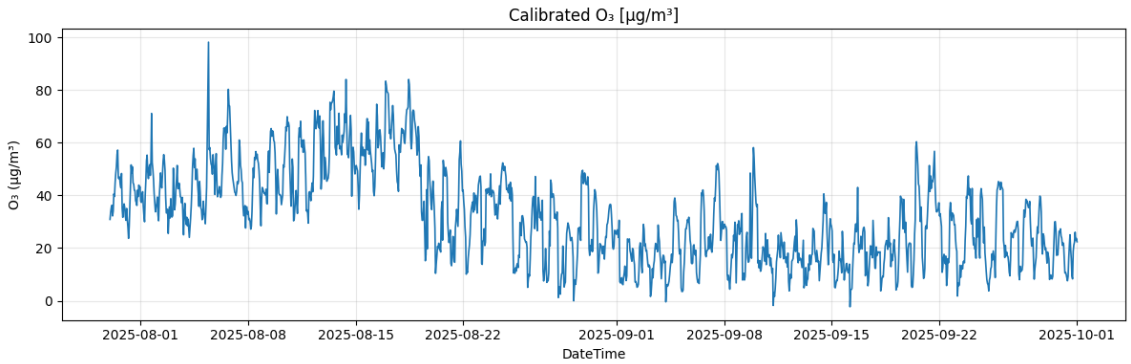

Figure 5.6: Time series of calibrated O_3 ($\mu g/m^3$) measured by the Monica sensor (PoliTO7) July 30-September 30, in a naturally ventilated room

Table 5.3: Hourly coverage, indoor median, and I/O ratio of PoliTO7

Period	**Hourly coverage**	**Indoor median** ($\mu g/m^3$)	**I/O ratio**
30 Jul-30 Sep	98.5 %	30.0	0.432
August 2025	97.7 %	41.5	0.500
September 2025	99.6 %	19.1	0.342

The daily profile in Figure 5.7 can be used to examine daily behavior. The first graph shows the daily profile of PoliTO6. there is an evident growth in the late morning (photochemical formation) and nighttime lows (absence of production and titration with NO), with hourly maximums generally between 100 and 120 $\mu g/m^3$ (Conil et al. 2025, Boleti et al. 2020). In this period, no exceedances of the information threshold (180 $\mu g/m^3$) are perceived; the peaks remain below it, suggesting intense but not extreme episodes, consistent with summer urban background conditions reported in long-term European observations (Conil et al. 2025). This outdoor dynamic constitutes the forcing that governs the indoor environment and clarifies the differences observed between the two sites: when the air exchange is limited (PoliTO1), the external wave is attenuated and dampened; when the ventilation is continuous (PoliTO7), the internal profile tracks the ambient cycle with reduced attenuation, showing higher I/O ratios and larger daytime amplitudes. The daily outdoor profile can be considered the reference, as its trend aligns with that of the summer cycle, featuring a rapid ascent from late morning and a maximum in the afternoon.

The profiles presented in Figure 5.7 indicate that the second graph (b) exhibits a damped pattern (5–10 $\mu g/m^3$), with a noticeably weakened afternoon peak. This behavior is consistent with expectations for conditions characterized by a low air exchange rate and significant wall losses, resulting in a reduced indoor-to-outdoor (I/O) ratio. The third graph (c) corresponds to the highly ventilated indoor environment (PoliTO7). The profile is in phase with the outdoor pattern, displaying an intermediate amplitude (approximately 20–45 $\mu g/m^3$) and a wide interquartile range during the central hours of the day. This last graph follows the daily profile of

the outdoor one (PoliTO6) with minimal delay and an hourly modulation of the air exchange rate. In general, the combination of daytime ventilation, indoor losses, and usage patterns results in slightly different profiles observed.

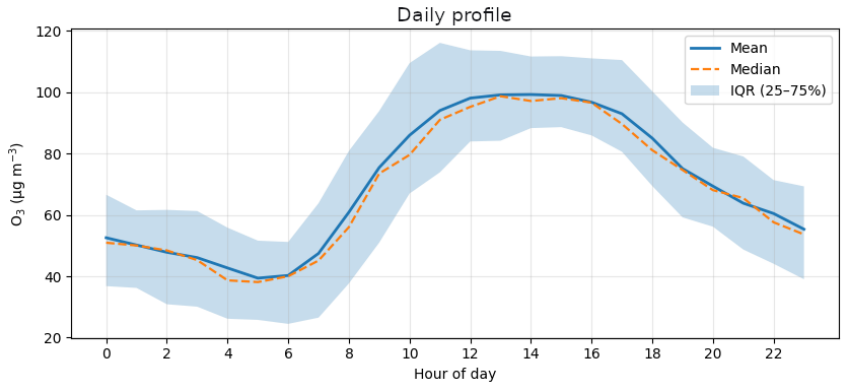

(a) Daily profile PoliTO6 (outdoor, roof site)

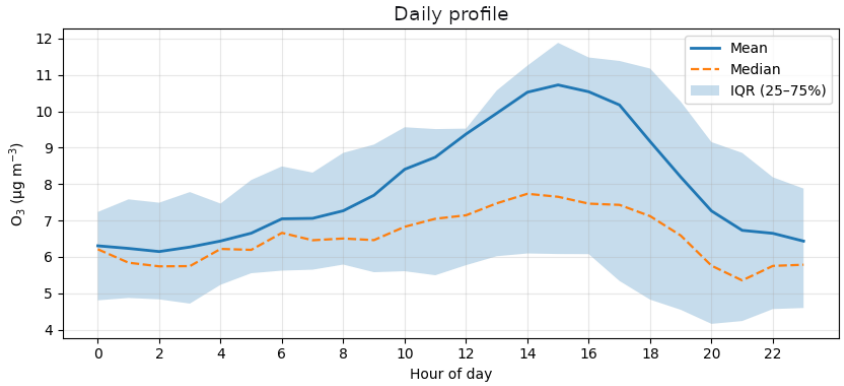

(b) Daily profile PoliTO1 (indoor, isolated non-ventilated room)

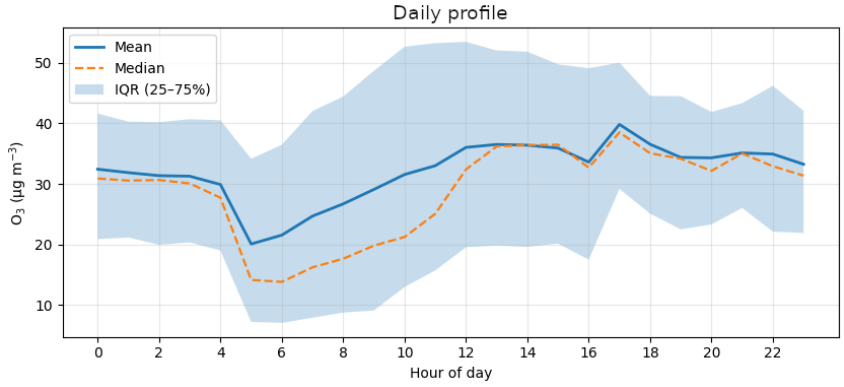

(c) Daily profile PoliTO7 (indoor, naturally ventilated room)

Figure 5.7: Daily profile of the Monica sensors July 30-September 30 at their deployment locations: PoliTO6 outdoor (roof site); PoliTO1 indoor, isolated non-ventilated room; PoliTO7 indoor, naturally ventilated room

5.2 Comparison with Legislative framework

The legislative restrictions for ozone levels under Directive 2008/50/EC and its revision in Directive 2024/2881 are presented in the introduction. The limits are examined in this section, and if there are any exceedances, the frequency of exceedances and their proximity to the alarm threshold are highlighted. In Figure 5.8, the maximum daily average for 8 hours (MDA8) of the outdoor ozone series is represented for the monitoring period. The daily 8-hour maximum (MDA8) is calculated in accordance with the WHO/EU convention by creating a rolling 8-hour mean from hourly data (local time), which necessitates at least 6 valid hours, and then selecting the daily maximum from those 8-hour means. The legislative thresholds are highlighted, and the threshold exceedance is indicated in Table 5.4. Considering that the reference target value of 120 $\mu g/m^3$ (MDA8) "shall not be exceeded on more than 25 days per year" as a three-year average (European Parliament and Council of the European Union 2008), the observation of 18 exceedance days over a short two-month window (63 valid days, 28.6 %) is strongly indicative of the threshold exceedance pressure during the peak season. Although extrapolating to a full year would be inappropriate given the seasonal bias of the sample, such a frequency concentrated in late summer would, if sustained over the ozone season, rapidly exhaust the annual allowance. For context, using the updated health benchmark introduced in Directive (EU) 2024/2881 (MDA8 = 100 $\mu g/m^3$), 33/63 days (52.4 %) exceeded 100 $\mu g/m^3$ in the same window, underscoring substantial health-relevant exposure even when legal compliance is judged by the 2008 metric.

Table 5.4: MDA8 exceedances for outdoor ozone in the analysis window (30 Jul-30 Sep 2025)

Threshold	Exceedance days	Total days	Share
MDA8 > 120 $\mu g/m^3$	18	63	28.6 %
MDA8 > 100 $\mu g/m^3$	33	63	52.4 %

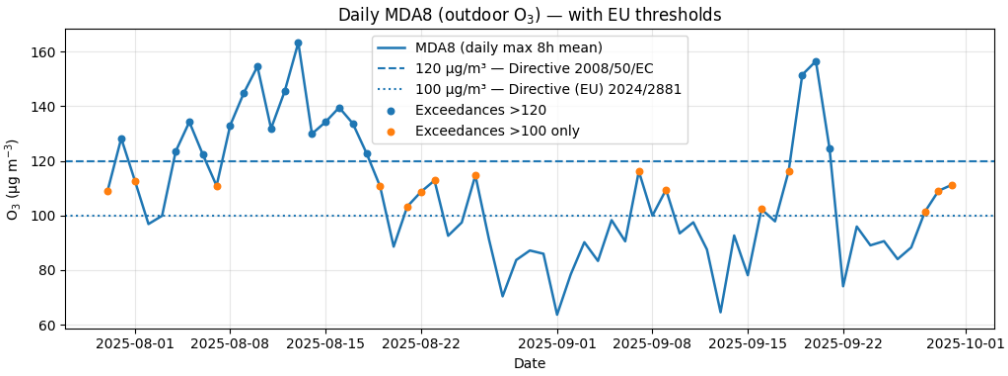

Figure 5.8: MDA8 O_3 ($\mu g/m^3$ compared with EU environmental limits)

For a complete analysis, Arpa Piemonte data are also considered, which record that the limits indicated by Directive 2008/50/EC were respected in 2 of 31 cross-country stations in the Piedmont area during the three-year period 2022-2024 (ARPA 2025). In 2024, the alarm threshold was not exceeded in any station, while the information threshold was exceeded in 3 out of 29 stations, with an overall number of episodes lower than in 2023 (4 compared to 34 last year) (ARPA 2025). Throughout the region, over the years, there has been a reduction in the number of exceedances, but not enough to comply with the limits of the legislation. This picture is complicated, considering that the limits of the new directive are even more stringent than the current ones. Currently, there is no mandatory recommendation for indoor ozone levels. Since most people spend their time indoors, indoor air quality and composition significantly influence people's health. Examining air quality in homes and workplaces is crucial since people often spend their time between the two. Globally, this kind of pollution is a major cause of premature mortality (Jacobson 2012). However, it is important to note that the WHO global air quality guidelines (Organization 2021), which underpin the Directive, apply globally to both outdoor and indoor environments (excluding occupational settings). For occupational settings, current EU directives do not establish specific limit values for ozone in the workplace; exposure assessments commonly refer to the ACGIH (American Conference of Governmental Industrial Hygienists) Threshold Limit Values (TLVs). In Table 5.5, all limits are indicated with a differ-

ence depending on the workload. Threshold Limit Values are airborne concentrations of chemicals that are believed to be safe for almost all workers to be exposed to on a daily basis for the duration of their working life (American Conference of Governmental Industrial Hygienists (ACGIH) 2025).

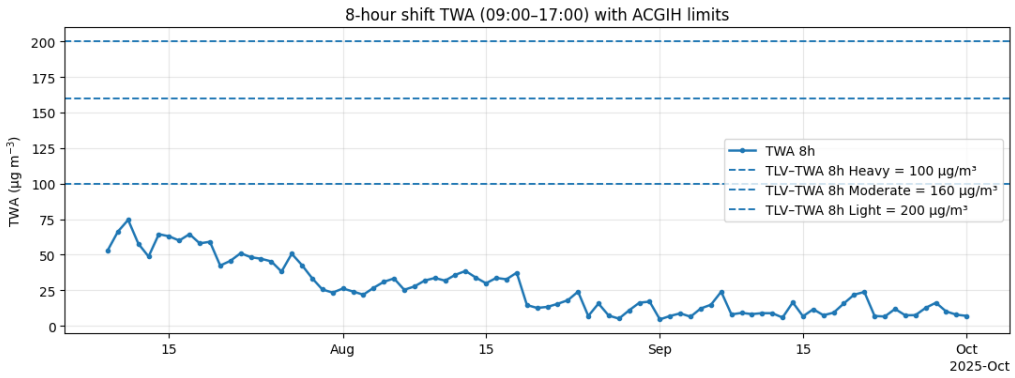

Figure 5.9: TWA 8 hours shift ACGIH occupational limits O_3 ($\mu g/m^3$)

Table 5.5: ACGIH limits for ozone in workplaces: ppm and mass concentration equivalents.

Entry	**Limit** (ppm)	**ACGIH** ($mg/m^3 \Rightarrow \mu g/m^3$)
TLV–TWA (8 h), heavy work	0.05	$0.10 \Rightarrow 100$
TLV–TWA (8 h), moderate work	0.08	$0.16 \Rightarrow 160$
TLV–TWA (8 h), light work	0.10	$0.20 \Rightarrow 200$
TLV–TWA (≤ 2 h), any workload	0.20	$0.39 \Rightarrow 390$

Notes. Mass concentrations follow ACGIH's display (rounded) and the ppm $\Leftrightarrow$ mg/m^3 conversion at 25 °C and 1 atm.

These limits are compared to the results for the PoliTO7 environment in Figure 5.9. The limits are met; however, the monitored room is rarely occupied. For most of the monitoring period, there were neither people present nor materials and activities typical of a working environment (e.g., cleaning agents, office equipment, consumer products) that release ozone-reactive compounds. In a standard working environment, human presence and routine activities introduce volatile organics and intermittent sources that can alter indoor ozone chemistry, leading to short-term increases and greater variability than observed here.

6

Interseasonal Evaluation: Winter Dataset

Politecnico di Torino purchased ten Monica devices for a monitoring campaign beginning in January 2025. The campaign is still ongoing, and the results will be presented in a scientific paper that is currently under review. Following the successful summer deployment, the analysis is extended to the January 2025 dataset to characterize ozone under winter meteorological conditions. To significantly reduce bias and improve agreement with reference analyzers, field calibration campaigns combined with supervised learning models must be applied to Monica data. Field calibration was carried out on the roof of the Politecnico di Torino Safety Laboratory. All 10 Monica devices were co-located on the roof alongside the reference analyzer.

The devices were positioned at the same height as the Serinus 10 reference analyzer. In accordance with Lewis and Edwards (2016) suggestions that multi-week co-location (ranging from two to three weeks) provides adequate variability for robust model fitting and short-term transferability, a two-week calibration window was considered, beginning on January 22 and ending on February 5, 2025. It is crucial to verify whether all ten of the Monica devices behaved consistently during the campaign and throughout these two weeks of calibration. Figure 6.1 displays the results. Nine sensors show excellent consistency between them during the

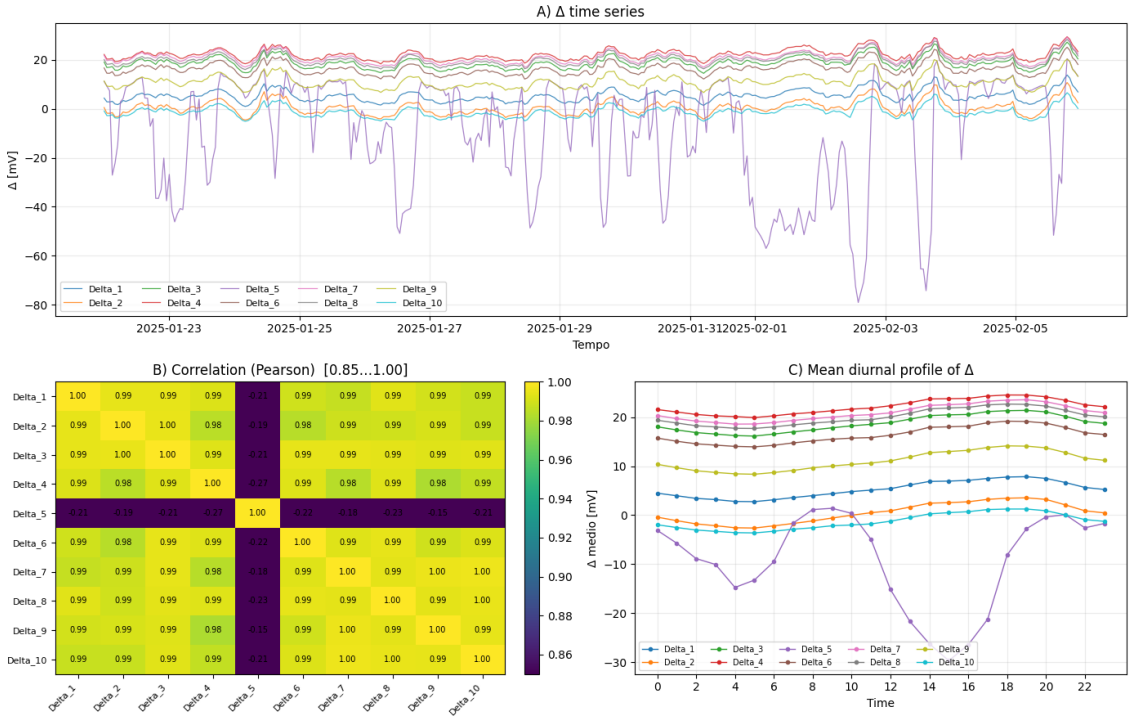

Figure 6.1: Correlation between all 10 Monica devices during the calibration period

calibration period, with high coherence (Pearson $r \geq 0.98$). Device 5 fails the consistency check and is excluded from the January 2025 calibration; it is subject to separate diagnostics. In panel A of Figure 6.1, the daily trends of 9 of 10 devices show a slight divergence in the sensitivity response of the individual sensors, probably due to different internal conditions, which can be compensated during the calibration procedure with reference to Serinus 10. Device 5, on the other hand, has large uncorrelated spikes and prolonged descents. The non-synchronous nature of the anomalies suggests an offset problem and not an environmental cause; therefore, the sensor was excluded from subsequent analyzes. The average daytime profile of delta in the C panel reveals a smooth and consistent pattern among 9 out of 10 devices; the fifth can be excluded from this analysis. The average daytime profile of the 9 devices shows a trend with a minimum at night and a maximum in the late afternoon; the reduced amplitude is consistent with winter conditions (low radiation, strong role of relative humidity, and night stability). The Serinus 10 UV photometric O_3 analyzer, compliant with EN 14625 and already presented

in the third chapter, is used as a reference instrument. Multiple linear regression (MLR) was used as a calibration model, with the procedure detailed in Chapter 4 applied uniformly to all data sets using Equation 4.1.

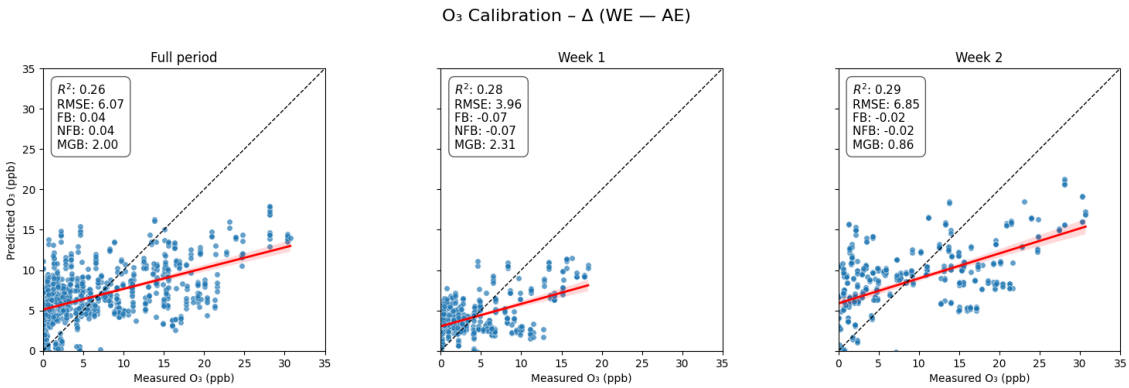

Figure 6.2: Calibration plots of the first Monica device located at the Politecnico di Torino site

In Figure 6.2, the calibration of the first device is shown. The calibrations for the 10 devices are represented in appendix C. The predictive capacity of the adopted model is limited, with R^2 being very low at approximately 0.26. Typical errors are modest and the average bias (FB/NFB) is close to zero, with slight over and under estimates depending on the week. It is clear that this calibration model is not suitable for the considered data series. It is necessary to understand the reasons for these results. Poor winter performance can be attributed to several factors. As seen in relation 2.5 in the steady state, the concentration of ozone can be approximated by

$$\chi_{O_3(g)} = \frac{j}{N_d k_1} \cdot \frac{\chi_{NO_2(g)}}{\chi_{NO(g)}} \tag{6.1}$$

Where χ is the volume mixing ratio (molecule of gas per molecule of dry air), j is the photolysis frequency of NO_2, k_1 is the bimolecular rate coefficient of ($NO + O_3 \longrightarrow NO_2 + O_2$) and N_d is the dry air concentration (molecules of dry air per cubic centimeter) (Jacobson 2012). This steady-state expression underestimates the observed ozone level, as it does not consider radical production and additional losses, but it remains a useful indicator for our analysis. In this report, the rela-

tionship of O_3 levels with photolysis and the ratio NO_2/NO is emphasized. Analyzing both photolysis and the NO_2/NO ratio, a different seasonal trend can be observed in winter compared to summer. In Figure 6.3 NO, NO_2 and NO_X are represented in January (winter) and July (summer). In January, NO is high; the NO_2/NO ratio is low around the unit. the high NO level causes a strong O_3 titration and a compressed ozone range; this compression lowers the signal-to-noise ratio and decreases the information content available to linear models. In July, the NO values are close to zero, and for most of the time, NO_2 follows NO_X. The NO_2/NO ratio is high due to the more intense summer photolysis; the conditions are favorable for higher O_3 levels. In addition to winter dynamics, the reasons for calibration failure may be related to the sensitivity of the low-cost sensor to temperature and relative humidity. This may require the insertion of dedicated predictors and corrections into the calibration to obtain satisfactory results.

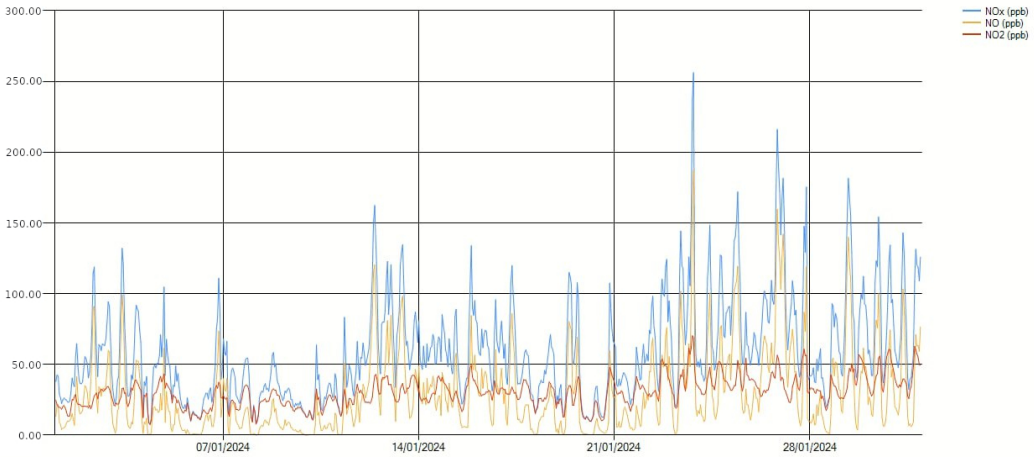

(a) January dataset

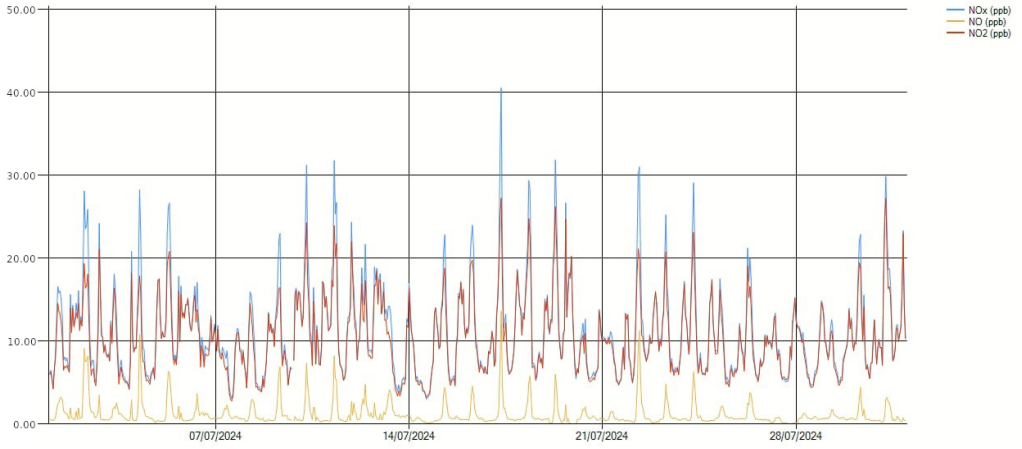

(b) July dataset

Figure 6.3: Time series of NO,NO_2 and NO_X in January (winter) and July (summer)

7

Conclusions

The aim of this work is to measure summer tropospheric ozone levels in indoor and outdoor environments using low-cost Monica sensors. Tropospheric ozone, unlike stratospheric ozone, can be harmful to both plants and animals, including humans. This is why it is important to monitor ozone levels to understand the repercussions on climate, human health, and agricultural production. Only the 25 % of the Earth's surface has ground-based data, and Low-cost sensors could represent a solution to expand the available dataset. A problem with low-cost sensors is calibration; in this work, it was decided to implement a field calibration by co-locating the 3 Monica sensors used with a reference instrument (Serinus 10). With two weeks of calibration, excellent results have been obtained. The calibration took place from 9 to 23 July 2025. The chosen model is that of multiple linear regression (MLR), considering the signal $\Delta = O_3We - O_3Ae$, the temperature, and the relative humidity. The results are excellent with $R^2 = 0.84–0.87$, RMSE = 5.8–6 ppb, and stability between August and September. This shows that, in summer, a linear calibration with microclimate correctors is sufficient for operational use. After calibration, the three Monica devices were placed in different environments. PoliTO6 stayed outside near the reference instrument (in the environmental safety laboratory), while PoliTO1 was placed in a closed laboratory, completely isolated, without ventilation and without activity. The last Monica, PoliTO7, was in a laboratory with a window that was always open but with no activ-

ity. PoliTO6 showed the typical summer daytime cycle, with many days exhibiting high MDA8 (maximum of the 8-hour average) Specifically, there were 18 of 63 days with limits above 120 $\mu g/m^3$ (target 2008/50/EC) and 33 days of 63 with values exceeding 100 $\mu g/m^3$ (target Directive 2024/2881). The information threshold of 180 $\mu g/m^3$ has never been exceeded, but the results obtained represent a signal of strong exposure during the peak season, even if the period is limited to the summer. From the PoliTO1 data, a median of 6.5 $\mu g/m^3$, an I/O ratio = 0.107 and a very attenuated daily profile are obtained. A low air exchange rate and a dynamic controlled mainly by surface deposition. The PoliTO7 data have a median of 30 $\mu g/m^3$, and a I/O ratio = 0.432. Values much higher than PoliTO1 are more closely coupled with the external trend, exhibiting high penetration and a high air exchange rate. A high I/O does not automatically equate to ”good ventilation” from a health point of view because it increases the ozone available for indoor reactions. However, in this environment, the absence of occupants and activities limits secondary chemistry. For indoor environments, there are no EU legal limits; references are made to WHO guidelines (WHO AQGs 100 $\mu g/m^3$ at 8 hours as a health reference) and, for occupational environments, to the TLV-TWA ACGIH, depending on the workload. In summer, the Monicas are suitable for space-time mapping and indoor/outdoor studies after a simple calibration in the field. However, in winter, the same procedure does not yield satisfactory results. This may be caused by the fact that the photochemical dynamics and the sensor’s sensitivity to temperature and relative humidity may require additional predictors, different models, and periodic rechecks as required by Directive 2024/2881. For future developments, it would be useful to expand the monitoring window to also include high-activity indoor sites that are more representative of offices and classrooms, where secondary chemistry is more relevant. The presence of indoor co-pollutants should also be evaluated to qualify secondary processes, especially in places with high indoor/outdoor ratios. On the winter calibration front, it is suggested to extend the co-localization period and enrich the model with photochemical indicators, or to try nonlinear calibration models implemented with periodic re-calibrations.

References

Acoem (2023). *Serinus 10 Ozone Analyzer - Technical Specification Sheet*. https://cdn.bfldr.com/Q3Z2TZY7/as/qgt8ht98s7vrh9rzmwv6q7xh/Acoem_Serinus_10_spec_sheet_20230426.

Agathokleous, E., A. De Marco, et al. (2022). "Air pollution and climate change threats to plant ecosystems". In: *Environmental Research* 212, p. 113420. DOI: 10.1016/j.envres.2022.113420.

Agathokleous, E., Z. Feng, et al. (2020). "Ozone affects plant, insect, and soil microbial communities: A threat to terrestrial ecosystems and biodiversity". In: *Science Advances* 6.33. DOI: 10.1126/sciadv.abc1176. URL: https://doi.org/10.1126/sciadv.abc1176.

Akritidis, D. et al. (2022). "A process-oriented evaluation of CAMS reanalysis ozone during tropopause folds over Europe for the period 2003-2018". In: *Atmospheric Chemistry and Physics* 22, pp. 6275–6289. DOI: 10.5194/acp-22-6275-2022.

American Conference of Governmental Industrial Hygienists (ACGIH) (2025). *TLV Chemical Substances Introduction*. URL: https://www.acgih.org/science/tlv-bei-guidelines/tlv-chemical-substances-introduction/.

Anav, A. et al. (2018). "Sensitivity of stomatal conductance to soil moisture: implications for tropospheric ozone". In: *Atmospheric Chemistry and Physics* 18, pp. 5747–5763. DOI: 10.5194/acp-18-5747-2018.

Archibald, A. T. et al. (2020). "On the changes in surface ozone over the twenty-first century: sensitivity to changes in surface temperature and chemical mech-

anisms". In: *Philosophical Transactions of the Royal Society A: Mathematical, Physical and Engineering Sciences* 378.2183. DOI: 10.1098/rsta.2019.0329.

ARPA Piemonte (2025a). *Qualità dell'aria — Dati*. Portale dei dati sulla qualità dell'aria. URL: https://aria.ambiente.piemonte.it/qualita-aria/dati.

— (Mar. 2025b). *Relazione sintetica anno 2024: Qualità dell'aria in Piemonte*. URL: https://www.arpa.piemonte.it/.../Relazione%20sintetica%20anno%202024.pdf.

Boleti, E. et al. (2020). "Temporal and spatial analysis of ozone concentrations in Europe based on timescale decomposition and a multi-clustering approach". In: *Atmospheric Chemistry and Physics* 20.14, pp. 9051–9066. DOI: 10.5194/acp-20-9051-2020. URL: https://doi.org/10.5194/acp-20-9051-2020.

Cagnazzo, C. et al. (2009). "Northern winter stratospheric temperature and ozone responses to ENSO inferred from an ensemble of Chemistry Climate Models". In: *Atmospheric Chemistry and Physics* 9, pp. 8935–8948. DOI: 10.5194/acp-9-8935-2009.

Conil, S. et al. (Mar. 2025). *Surface Ozone: Seasonal cycles, trends and events, a new perspective from the OPE station in France over the 2012–2023 period*. DOI: 10.5194/egusphere-2025-148. URL: https://doi.org/10.5194/egusphere-2025-148.

Cui, H. et al. (2021). "A new calibration system for low-cost Sensor Network in air quality monitoring: a four-stage calibration covering the full life cycle". In: *Environmental Technology & Innovation* 24, p. 101094. DOI: 10.1016/j.eti.2021.101094.

De Vito, S., A. Del Giudice, et al. (2023). "Correlating Air Pollution Concentrations and Vehicular Emissions in an Italian Roadway Tunnel by Means of Low Cost Sensors". In: *Atmosphere* 14.4, p. 679. DOI: 10.3390/atmos14040679.

De Vito, S., E. Esposito, et al. (2021). "Crowdsensing IoT Architecture for Pervasive Air Quality and Exposome Monitoring: Design, Development, Calibration, and Long-Term Validation". In: *Sensors* 21.15, p. 5219. DOI: 10.3390/s21155219.

Dewan, S. and A. Lakhani (2022). “Tropospheric ozone and its natural precursors impacted by climatic changes in emission and dynamics”. In: *Frontiers in Environmental Science* 10, p. 1007942. DOI: 10.3389/fenvs.2022.1007942.

Doherty, R. M. et al. (2013). “Impacts of climate change on surface ozone and intercontinental ozone pollution: A multi-model study”. In: *Journal of Geophysical Research: Atmospheres* 118.9, pp. 3744–3763. DOI: 10.1002/jgrd.50266.

Donzelli, G. and M. M. Suarez-Varela (2024). “Tropospheric Ozone: A Critical Review of the Literature on Emissions, Exposure, and Health Effects”. In: *Atmosphere* 15.7, p. 779. DOI: 10.3390/atmos15070779. URL: https://www.mdpi.com/2073-4433/15/7/779.

European Parliament and Council of the European Union (May 21, 2008). *Directive 2008/50/EC of the European Parliament and of the Council of 21 May 2008 on ambient air quality and cleaner air for Europe*. URL: https://eur-lex.europa.eu/legal-content/EN/TXT/PDF/?uri=CELEX:02008L0050-20150918.

— (Oct. 23, 2024). *Directive (EU) 2024/2881 of the European Parliament and of the Council of 23 October 2024 on ambient air quality and cleaner air for Europe (recast)*. OJ L 2024/2881, 20 Nov 2024. URL: https://eur-lex.europa.eu/legal-content/EN/TXT/PDF/?uri=OJ:L_202402881.

Fischer, E. V. et al. (2014). “Atmospheric peroxyacetyl nitrate (PAN): A global budget and source attribution”. In: *Atmospheric Chemistry and Physics* 14.5, pp. 2679–2698. DOI: 10.5194/acp-14-2679-2014.

Garfinkel, C. I. et al. (2018). “Nonlinear response of tropical lower-stratospheric temperature and water vapor to ENSO”. In: *Atmospheric Chemistry and Physics* 18, pp. 4597–4615. DOI: 10.5194/acp-18-4597-2018.

Geddes, J. A., S. E. Pusede, and A. Y. H. Wong (2022). “Changes in the Relative Importance of Biogenic Isoprene and Soil NOx Emissions on Ozone Concentrations in Nonattainment Areas of the United States”. In: *Journal of Geophysical Research: Atmospheres* 127.13, e2021JD036361. DOI: 10.1029/2021JD036361.

Gedney, N. et al. (2019). “Significant feedbacks of wetland methane release on climate change and the causes of their uncertainty”. In: *Environmental Research Letters* 14.8, p. 084027. DOI: 10.1088/1748-9326/ab2726.

Geyh A. S. a+-nd Xue, J., H. Özkaynak, and J. D. Spengler (2000). “The Harvard Southern California Chronic Ozone Exposure Study: assessing ozone exposure of grade-school-age children in two Southern California communities”. In: *Environmental Health Perspectives* 108.3, pp. 265–270. DOI: 10.1289/ehp.00108265.

Hardacre, C., O. Wild, and L. Emberson (2015). “An evaluation of ozone dry deposition in global scale chemistry climate models”. In: *Atmospheric Chemistry and Physics* 15, pp. 6419–6436. DOI: 10.5194/acp-15-6419-2015.

Hope, P. et al. (2017). “Time-varying spectral characteristics of ENSO over the Last Millennium”. In: *Climate Dynamics* 49, pp. 1705–1727. DOI: 10.1007/s00382-016-3393-z. URL: https://link.springer.com/article/10.1007/s00382-016-3393-z.

Hui, K. et al. (2023). “A review of the factors affecting the emission of the ozone chemical precursors VOCs and NOx from the soil”. In: *Environment International* 172, p. 107799. DOI: 10.1016/j.envint.2023.107799.

Jacobson, M. Z. (2012). *Air Pollution and Global Warming: History, Science, and Solutions*. 2nd ed. New York: Cambridge University Press. ISBN: 978-1107691155.

Jiang, Z. et al. (2016). “Ozone export from East Asia: The role of PAN”. In: *Journal of Geophysical Research: Atmospheres* 121.11, pp. 6555–6563. DOI: 10.1002/2016JD024952.

Kang, D. et al. (2020). “Significant ground-level ozone attributed to lightning-induced nitrogen oxides during summertime over the Mountain West States”. In: *npj Climate and Atmospheric Science* 3.1, pp. 1–7. DOI: 10.1038/s41612-020-0108-2.

Kavassalis, S. C. and J. G. Murphy (2017). “Understanding ozone-meteorology correlations: A role for dry deposition”. In: *Geophysical Research Letters* 44.16, pp. 8559–8568. DOI: 10.1002/2016GL071791.

Knowland, K. E. et al. (2017). “The influence of mid-latitude cyclones on European background surface ozone”. In: *Atmospheric Chemistry and Physics* 17.20, pp. 12421–12447. DOI: 10.5194/acp-17-12421-2017.

Leighton, P. A. (1961). *Photochemistry of Air Pollution*. New York: Academic Press.

Lewis, A. and P. Edwards (2016). *Validate Air Quality Low-Cost Sensor Evaluation Report*. Tech. rep. JRC90463. European Commission, Joint Research Centre (JRC). URL: https://publications.jrc.ec.europa.eu/repository/handle/JRC90463.

Liu, G. et al. (2015). “Ozone chemistry on human skin lipids produces highly irritating oxidation products”. In: *Proceedings of the National Academy of Sciences of the USA* 112, pp. 6568–6575. DOI: 10.1073/pnas.1503073112.

Lu, X., X. Ye, et al. (2021). “The underappreciated role of agricultural soil nitrogen oxide emissions in ozone pollution regulation in North China”. In: *Nature Communications* 12. DOI: 10.1038/s41467-021-25147-9.

Lu, X., L. Zhang, and L. Shen (2019). “Meteorology and Climate Influences on Tropospheric Ozone: a Review of Natural Sources, Chemistry, and Transport Patterns”. In: *Current Pollution Reports* 5.4, pp. 238–260. DOI: 10.1007/s40726-019-00118-3.

Monks, P. S. et al. (2015). “Tropospheric ozone and its precursors from the urban to the global scale from air quality to short-lived climate forcer”. In: *Atmospheric Chemistry and Physics* 15.15, pp. 8889–8973. DOI: 10.5194/acp-15-8889-2015.

Mousavinezhad, S. et al. (2023). “Surface ozone trends and related mortality across the climate regions of the contiguous United States during the most recent climate period, 1991-2020”. In: *Atmospheric Environment* 300, p. 119693. DOI: 10.1016/j.atmosenv.2023.119693. URL: https://www.sciencedirect.com/science/article/abs/pii/S135223102300119X.

Müller, R. (2012). *Stratospheric Ozone Depletion and Climate Change*. Cambridge: Royal Society of Chemistry.

Nazaroff, W. W. and C. J. Weschler (2022). "Indoor ozone: Concentrations and influencing factors". In: *Indoor Air* 32.1, e12942. DOI: 10.1111/ina.12942.

Ni, J. et al. (2024). "Surface ozone in global cities: A synthesis of basic features, exposure risk, and leading meteorological driving factors". In: *Geography and Sustainability* 5.1, pp. 64–76. DOI: 10.1016/j.geosus.2023.09.008.

Nowack, P. J. et al. (2017). "On the role of ozone feedback in the ENSO amplitude response under global warming". In: *Geophysical Research Letters* 44.16, pp. 3858–3866. DOI: 10.1002/2016GL072418.

Organization, W. H. (Sept. 2021). *New WHO Global Air Quality Guidelines aim to save millions of lives from air pollution*. https://www.who.int/news/item/22-09-2021-new-who-global-air-quality-guidelines-aim-to-save-millions-of-lives-from-air-pollution. News release.

Peiro, H. et al. (2018). "Multi-year assimilation of IASI and MLS ozone retrievals: variability of tropospheric ozone over the tropics in response to ENSO". In: *Atmospheric Chemistry and Physics* 18, pp. 6939–6958. DOI: 10.5194/acp-18-6939-2018.

Peñuelas, J. and M. Staudt (2010). "BVOCs and global change". In: *Trends in Plant Science* 15.3, pp. 133–144. DOI: 10.1016/j.tplants.2009.12.005.

Price, C., J. Penner, and M. Prather (1997). "NOx from lightning 1. Global distribution based on lightning physics". In: *Journal of Geophysical Research: Atmospheres* 102.5, pp. 5929–5941. DOI: 10.1029/96JD03504.

Regione Piemonte (Apr. 2019). *Piano Regionale per la Qualità dell'Aria (PRQA). Allegato 1*. Rapporto tecnico. Torino, Italia: Regione Piemonte. URL: https://www.regione.piemonte.it/web/sites/default/files/media/documenti/2019-04/prqa_allegato1_def.pdf (visited on 11/10/2025).

Rinnan, R. and C. N. Albers (2020). "Soil Uptake of Volatile Organic Compounds: Ubiquitous and Underestimated?" In: *Journal of Geophysical Research: Biogeosciences* 125.6, e2020JG005773. DOI: 10.1029/2020JG005773.

Romer, P. S. et al. (2018). “Effects of temperature-dependent NOx emissions on continental ozone production”. In: *Atmospheric Chemistry and Physics* 18.4, pp. 2601–2614. DOI: 10.5194/acp-18-2601-2018.

Schneidemesser, E. von et al. (2015). “Chemistry and the Linkages between Air Quality and Climate Change”. In: *Chemical Reviews* 115.10, pp. 3856–3897. DOI: 10.1021/acs.chemrev.5b00089. URL: https://doi.org/10.1021/acs.chemrev.5b00089.

Sha, T. et al. (2021). “Impacts of Soil NOx Emission on O3 Air Quality in Rural California”. In: *Environmental Science & Technology* 55.10, pp. 7113–7122. DOI: 10.1021/acs.est.0c06834.

Shen, L., L. J. Mickley, and A. P. K. Tai (2015). “Influence of synoptic patterns on surface ozone variability over the eastern United States from 1980 to 2012”. In: *Atmospheric Chemistry and Physics* 15, pp. 10925–10938. DOI: 10.5194/acp-15-10925-2015.

Sillman, S. and D. He (2002). “Some theoretical results concerning O3-NOx-VOC chemistry and NOx-VOC indicators”. In: *Journal of Geophysical Research: Atmospheres* 107. DOI: 10.1029/2001JD001123.

Solberg, S. et al. (2008). “European surface ozone in the extreme summer 2003”. In: *Journal of Geophysical Research: Atmospheres* 113.D07, p. D07307. DOI: 10.1029/2007JD009098.

Solerzia S.r.l. (2025). *Manuale d’uso MoNiCa — Dispositivo per il monitoraggio della qualità dell’aria*. Rev. 1.0. Manuale tecnico. Politecnico di Torino.

Spinelle, L., M. Gerboles, G. Kok, et al. (2015). “Field calibration of a cluster of low-cost sensors for air quality monitoring. Part A: Ozone and nitrogen dioxide”. In: *Sensors and Actuators B: Chemical* 215, pp. 249–257. DOI: 10.1016/j.snb.2015.06.049.

Spinelle, L., M. Gerboles, M. G. Villani, et al. (2017). “Field calibration of a cluster of low-cost commercially available sensors for air quality monitoring. Part B: NO, CO and CO_2”. In: *Sensors and Actuators B: Chemical* 238, pp. 706–715. DOI: 10.1016/j.snb.2016.07.036.

Talukdar, R. K. et al. (1995). “Investigation of the loss processes for peroxyacetyl nitrate in the atmosphere: UV photolysis and reaction with OH”. In: *Journal of Geophysical Research: Atmospheres* 100.D7, pp. 14163–14173. DOI: 10.1029/95JD00545.

Tarasick, D. et al. (2019). “Tropospheric ozone assessment report: Tropospheric ozone from 1877 to 2016, observed levels, trends and uncertainties”. In: *Elementa: Science of the Anthropocene* 7, p. 39. DOI: 10.1525/elementa.376. URL: https://doi.org/10.1525/elementa.376.

The Royal Society (2008). *Ground-level ozone in the 21st century: future trends, impacts and policy implications*. Science Policy Report 15/08. Royal Society.

Trowbridge, A. M., P. C. Stoy, and R. P. Phillips (2020). “Soil Biogenic Volatile Organic Compound Flux in a Mixed Hardwood Forest: Net Uptake at Warmer Temperatures and the Importance of Mycorrhizal Associations”. In: *Journal of Geophysical Research: Biogeosciences* 125.4, e2019JG005479. DOI: 10.1029/2019JG005479.

U.S. Environmental Protection Agency (2009). *Assessment of the Impacts of Global Change on Regional U.S. Air Quality: A Synthesis of Climate Change Impacts on Ground-Level Ozone*. URL: https://www.epa.gov.

Wang, T. et al. (2017). “Ozone pollution in China: A review of concentrations, meteorological influences, chemical precursors, and effects”. In: *Science of the Total Environment* 575, pp. 1582–1596. DOI: 10.1016/j.scitotenv.2016.10.081.

Weber, J. et al. (2022). *Chemistry-driven changes strongly influence climate forcing from vegetation emissions*. Research Square preprint. DOI: 10.21203/rs.3.rs-1646168/v1. URL: https://www.researchsquare.com/article/rs-1646168/v1.

Weng, H. et al. (2020). “Global high-resolution emissions of soil NOx, sea salt aerosols, and biogenic volatile organic compounds”. In: *Scientific Data* 7. DOI: 10.1038/s41597-020-0488-5.

Weschler, C. J. and H. C. Shields (2000). “The influence of ventilation on reactions among indoor pollutants: modeling and experimental observations”. In: *Indoor Air* 10.2, pp. 92–100. DOI: 10.1034/j.1600-0668.2000.010004269.x.

Wesely, M. L. (1989). “Parameterization of surface resistances to gaseous dry deposition in regional-scale numerical models”. In: *Atmospheric Environment* 23.6, pp. 1293–1304. ISSN: 0004-6981. DOI: 10.1016/0004-6981(89)90153-4.

World Health Organization (2006). *Air quality guidelines for particulate matter, ozone, nitrogen dioxide and sulfur dioxide: Global update 2005*. WHO-SDE-PHE-OEH-06.02. Available at https://www.who.int/publications/i/item/WHO-SDE-PHE-OEH-06-02. Geneva: World Health Organization.

— (2021). *WHO global air quality guidelines: particulate matter ($PM_{2.5}$ and PM_{10}), ozone, nitrogen dioxide, sulfur dioxide and carbon monoxide*. Geneva, Switzerland: World Health Organization. ISBN: 978-92-4-003422-8. URL: https://www.who.int/publications/i/item/9789240034228.

Xiong, X. et al. (2022). “Satellite observation of stratospheric intrusions and ozone transport using CrIS on SNPP”. In: *Atmospheric Environment* S, pp. 5747–5763. DOI: 10.1016/j.atmosenv.2022.1352231022000218.

Xue, L. et al. (2021). “ENSO and Southeast Asian biomass burning modulate subtropical trans-Pacific ozone transport”. In: *National Science Review* 8.6. DOI: 10.1093/nsr/nwaa132.

Yu, H. et al. (2021). “Potential of Climate Change and Herbivory to Affect the Release and Atmospheric Reactions of BVOCs from Boreal and Subarctic Forests”. In: *Molecules* 26.8, p. 2283. DOI: 10.3390/molecules26082283.

Zhang, L. et al. (2011). “Impacts of 2006 Indonesian fires and dynamics on tropical upper tropospheric carbon monoxide and ozone”. In: *Atmospheric Chemistry and Physics* 11, pp. 10929–10946. DOI: 10.5194/acp-11-10929-2011.

A

Ambient characteristics

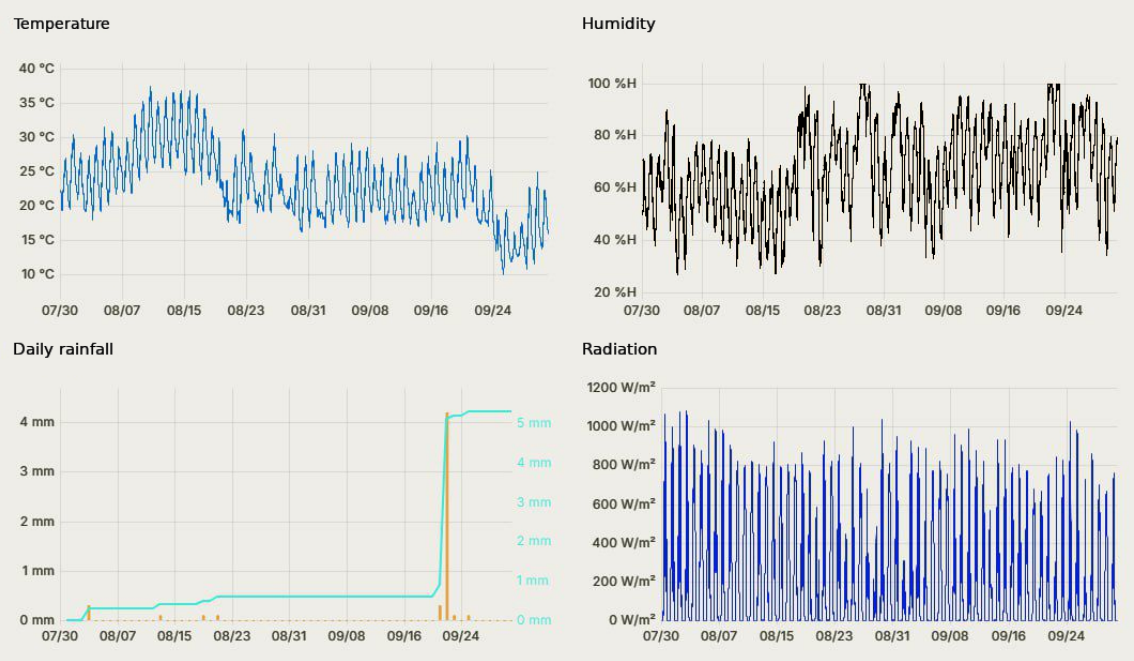

Figure A.1: Temperature, relative humidity, daily rainfall, radiation for August and September 2025

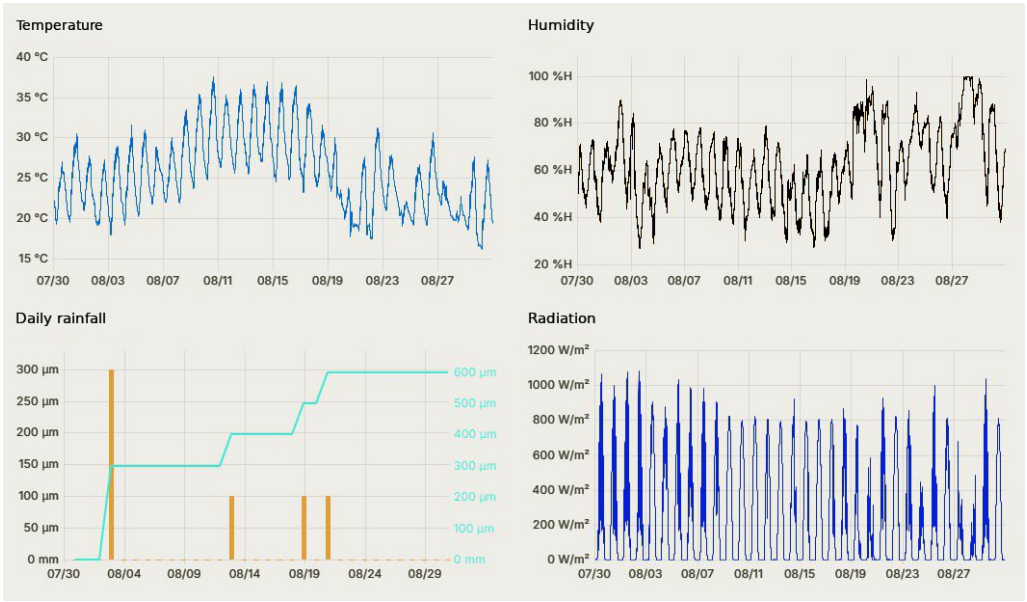

(a) August

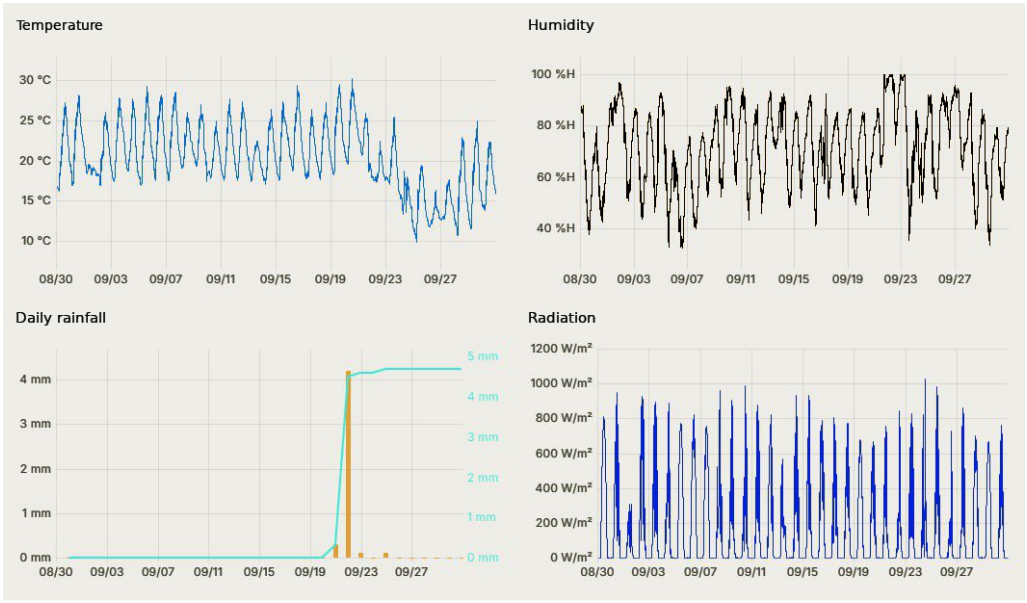

(b) September

Figure A.2: August and September 2025 trend

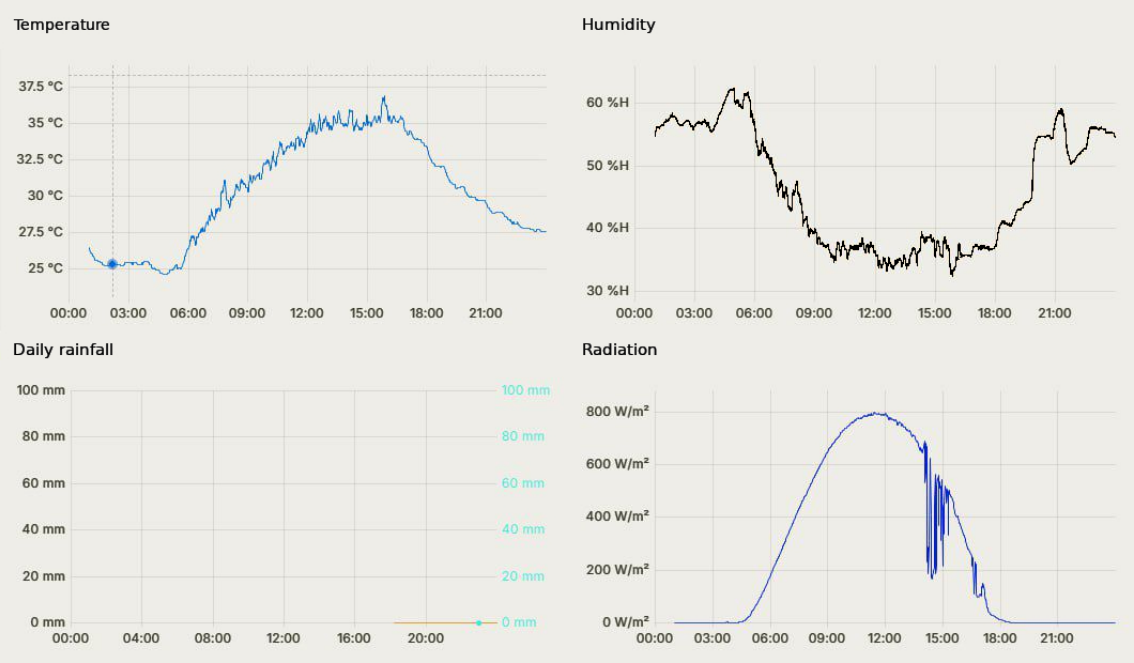

Figure A.3: Example of daily temperature, relative humidity, rainfall and radiation

B

Monthly and weekly ozone trend

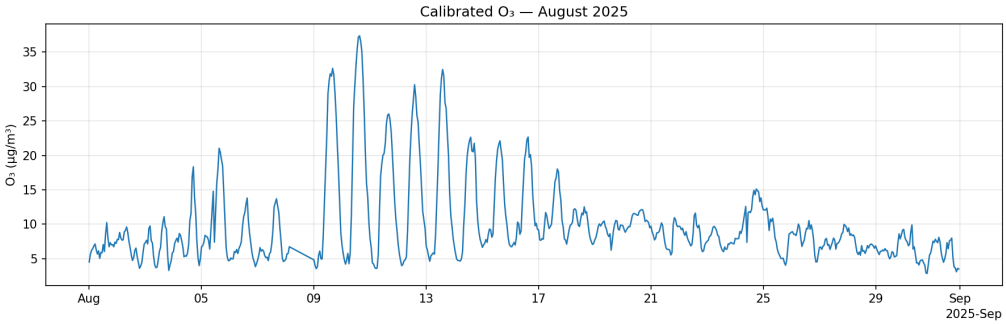

(a) August

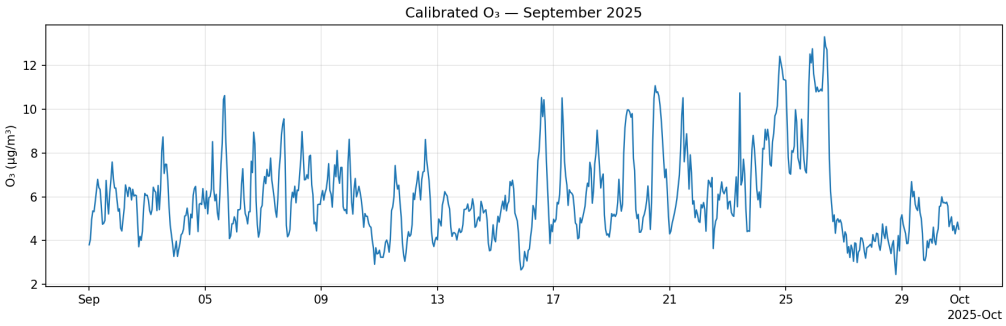

(b) September

Figure B.1: O_3 August and September trend PoliTO1

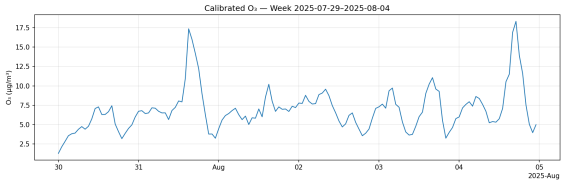

(a) week 1 (29/07 - 04/08)

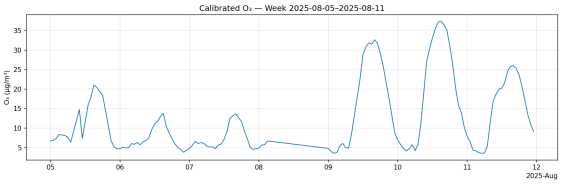

(b) week 2 (05/08 - 11/08)

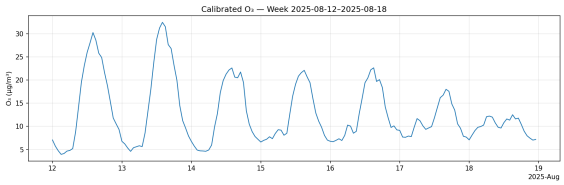

(c) week 3 (12/08 - 18/08)

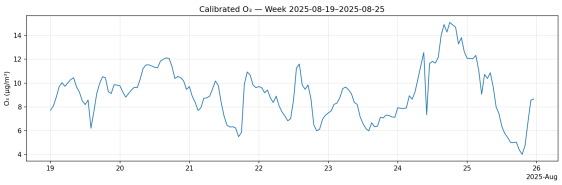

(d) week 4 (19/08 - 25/08)

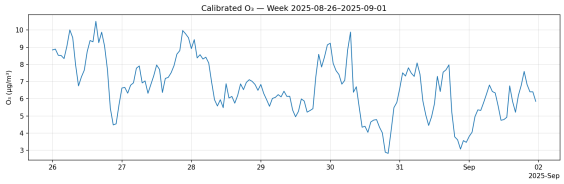

(e) week 5 (26/08 - 01/09)

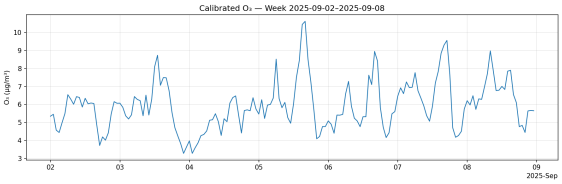

(f) week 6 (02/09 - 08/09)

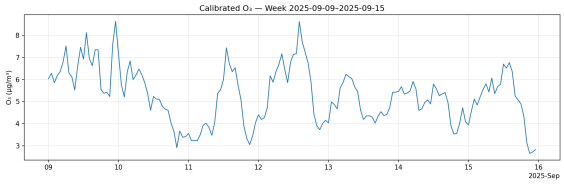

(g) week 7 (09/09 - 15/09)

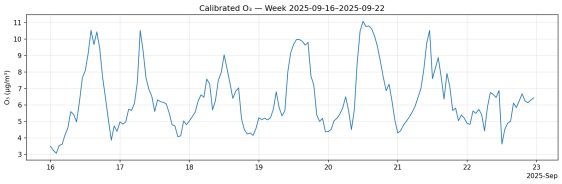

(h) week 8 (16/09 - 22/09)

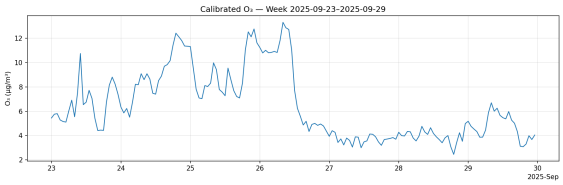

(i) week 9 (23/09 - 29/09)

Figure B.2: O_3 weekly trend PoliTO1

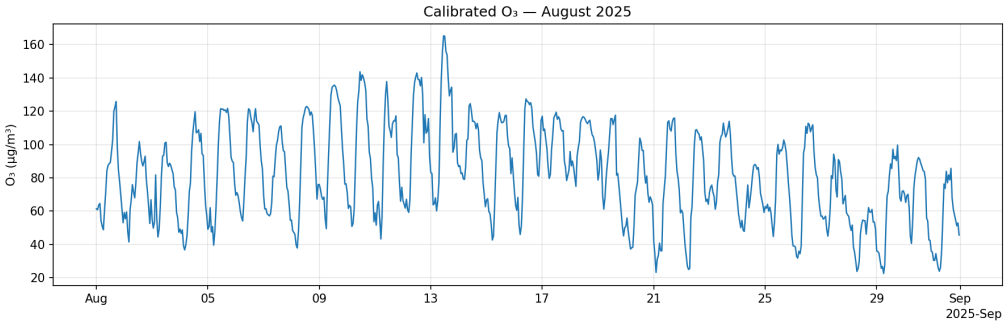

(a) August

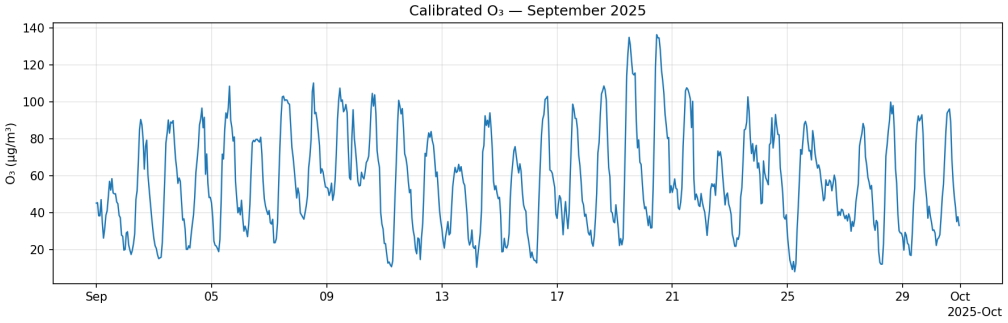

(b) September

Figure B.3: O_3 August and September trend PoliTO6

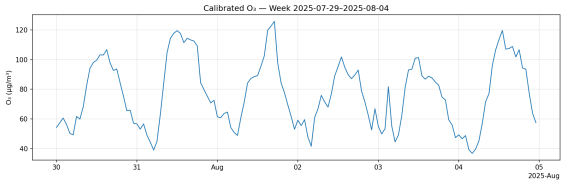

(a) week 1 (29/07 - 04/08)

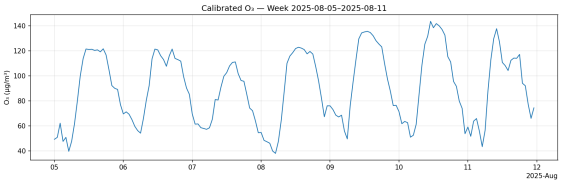

(b) week 2 (05/08 - 11/08)

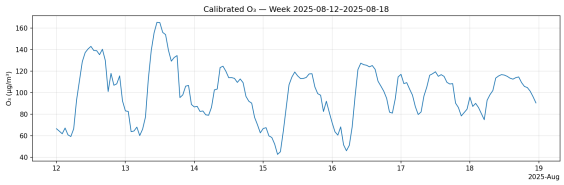

(c) week 3 (12/08 - 18/08)

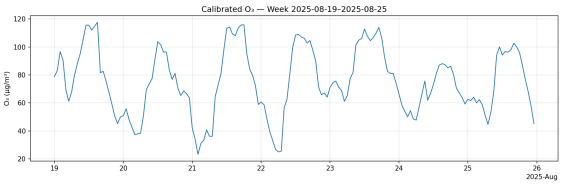

(d) week 4 (19/08 - 25/08)

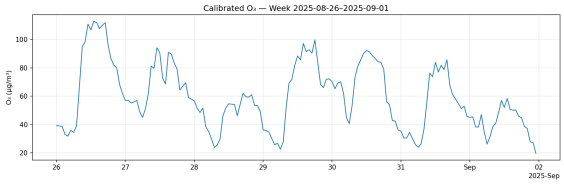

(e) week 5 (26/08 - 01/09)

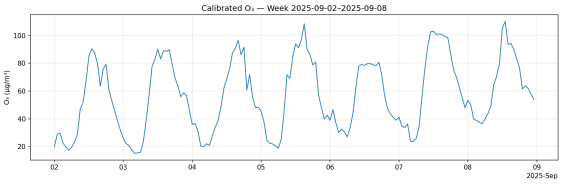

(f) week 6 (02/09 - 08/09)

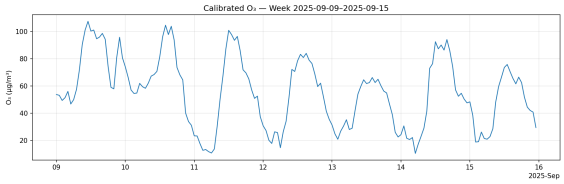

(g) week 7 (09/09 - 15/09)

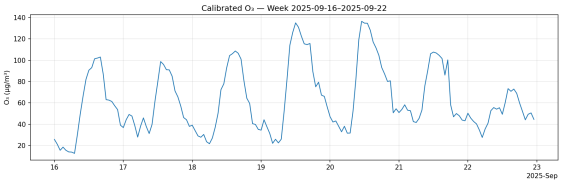

(h) week 8 (16/09 - 22/09)

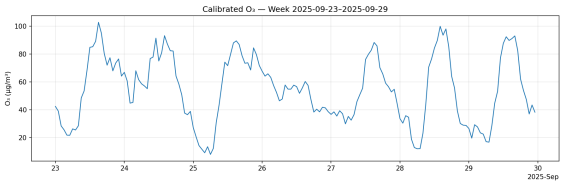

(i) week 9 (23/09 - 29/09)

Figure B.4: O_3 weekly trend PoliTO6

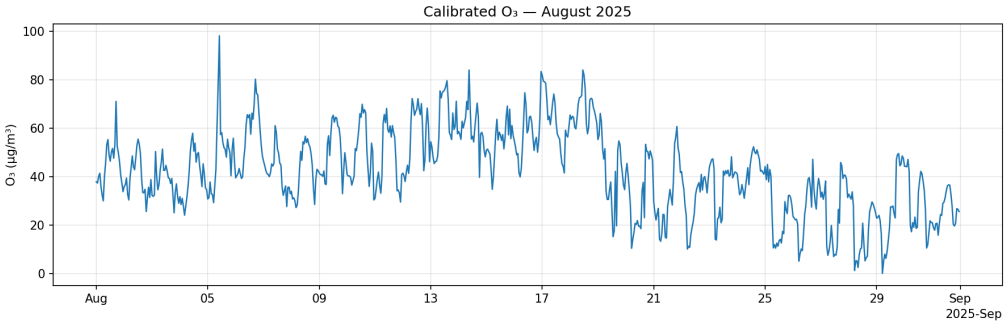

(a) August

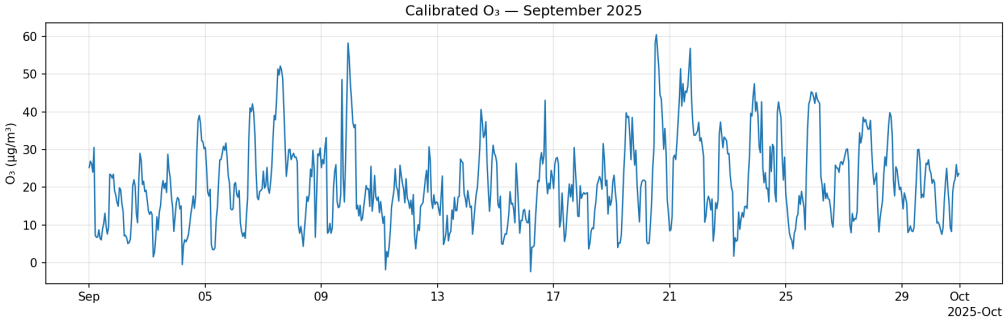

(b) September

Figure B.5: O_3 August and September trend PoliTO7

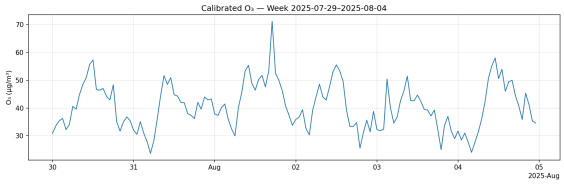

(a) week 1 (29/07 - 04/08)

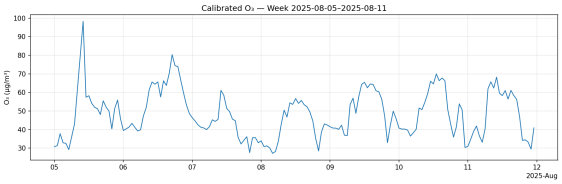

(b) week 2 (05/08 - 11/08)

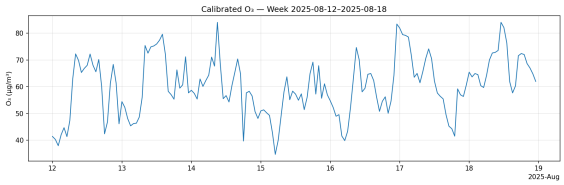

(c) week 3 (12/08 - 18/08)

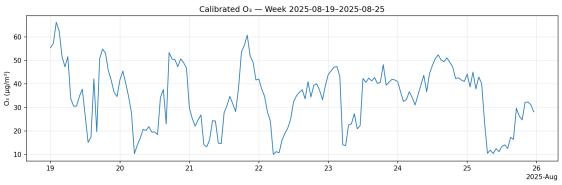

(d) week 4 (19/08 - 25/08)

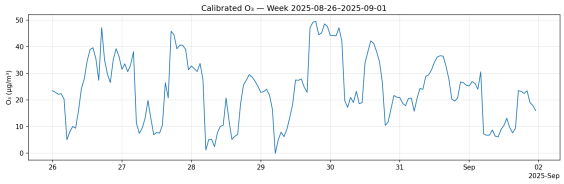

(e) week 5 (26/08 - 01/09)

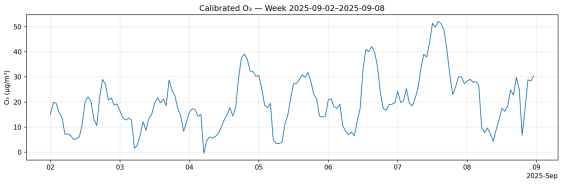

(f) week 6 (02/09 - 08/09)

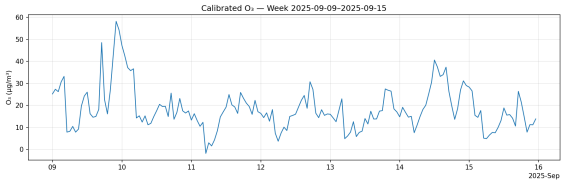

(g) week 7 (09/09 - 15/09)

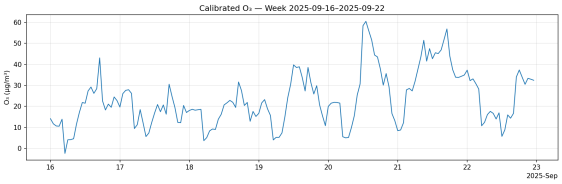

(h) week 8 (16/09 - 22/09)

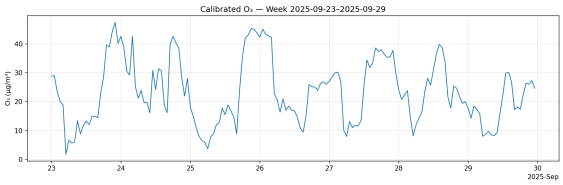

(i) week 9 (23/09 - 29/09)

Figure B.6: O_3 weekly trend PoliTO7

C

Supplementary material on winter calibration

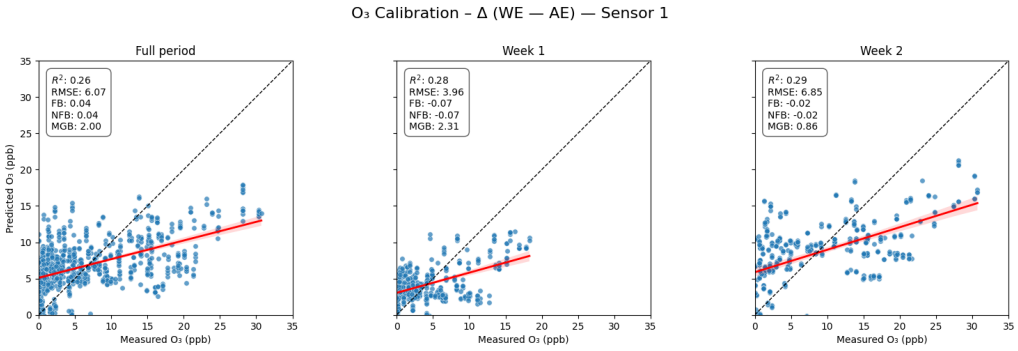

Figure C.1: Calibration plot - PoliTO1

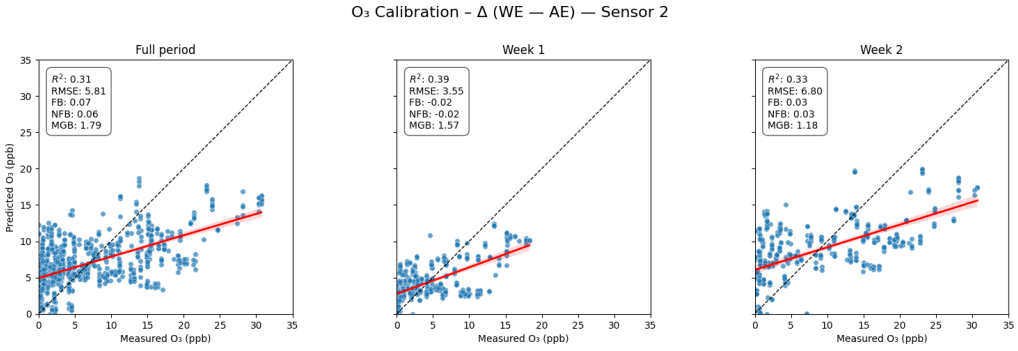

Figure C.2: Calibration plot - PoliTO2

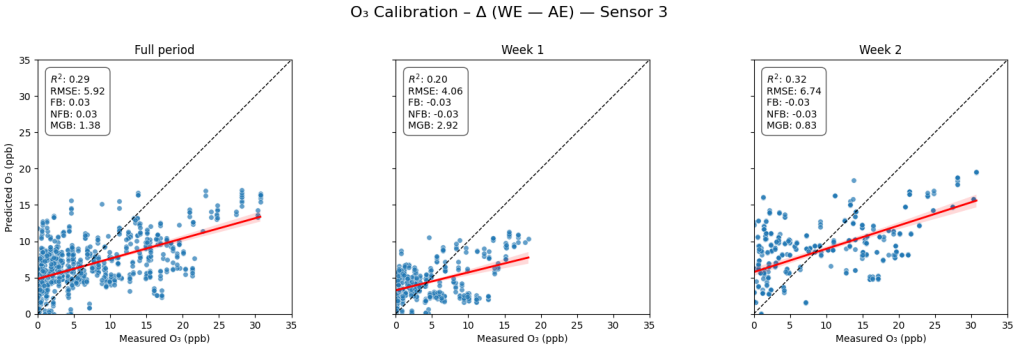

Figure C.3: Calibration plot - PoliTO3

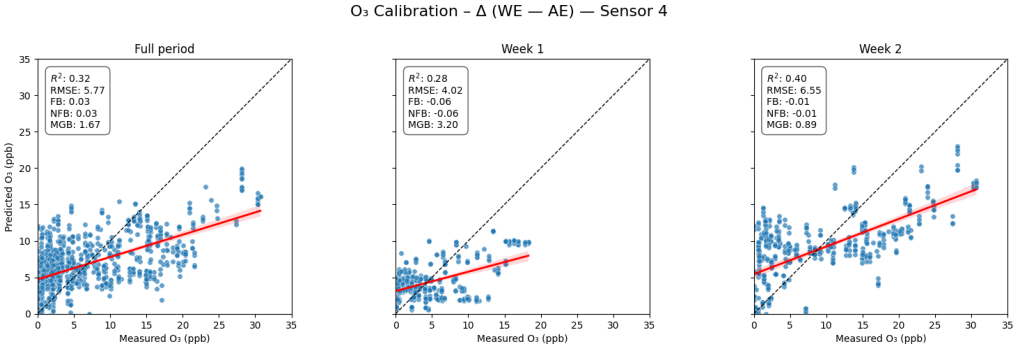

Figure C.4: Calibration plot - PoliTO4

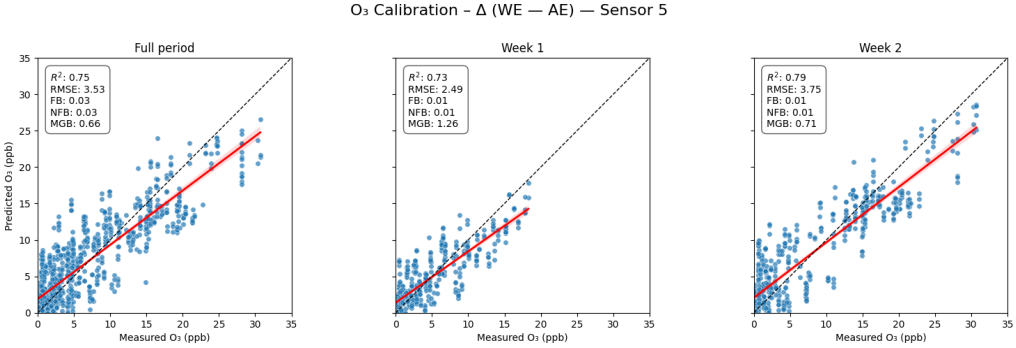

Figure C.5: Calibration plot - PoliTO5 (excluded from the analysis)

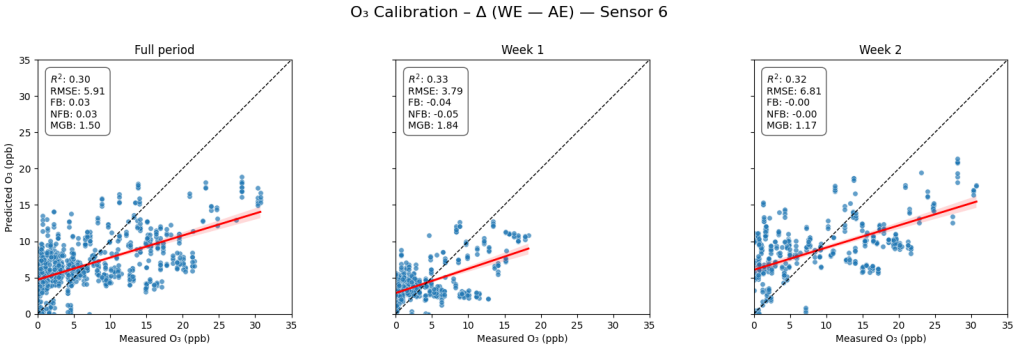

Figure C.6: Calibration plot - PoliTO6

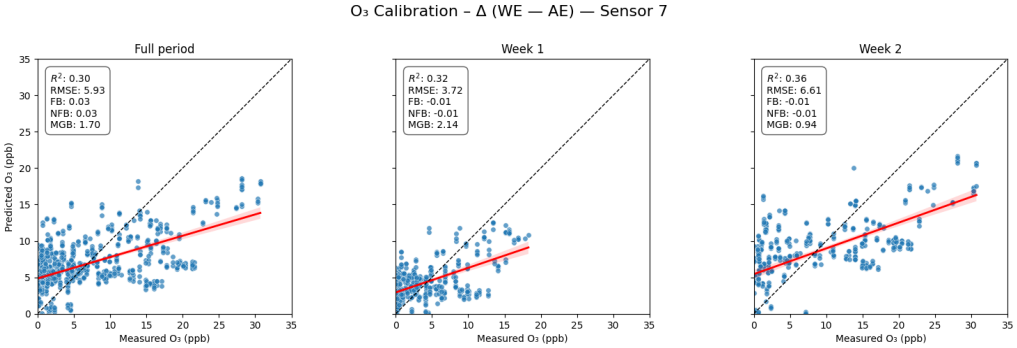

Figure C.7: Calibration plot - PoliTO7

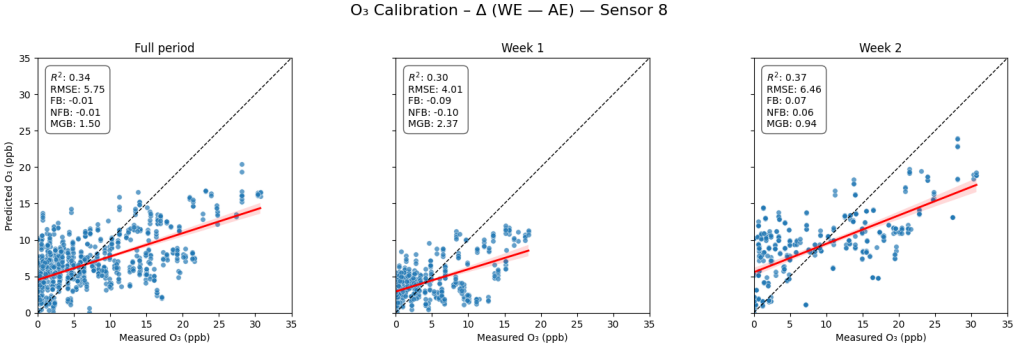

Figure C.8: Calibration plot - PoliTO8

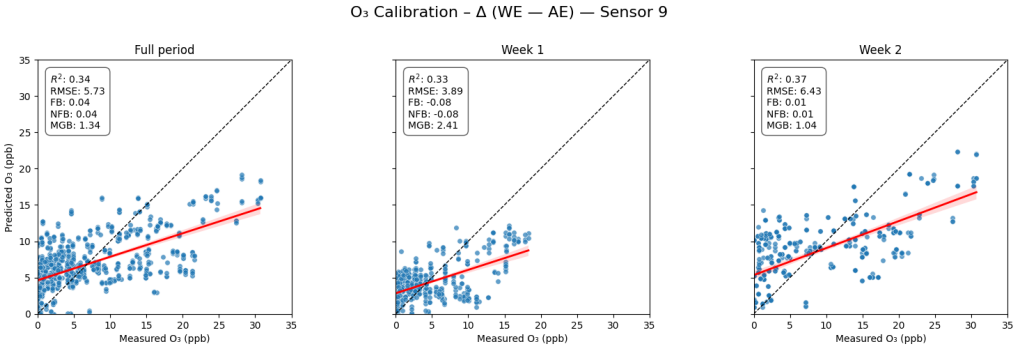

Figure C.9: Calibration plot - PoliTO9

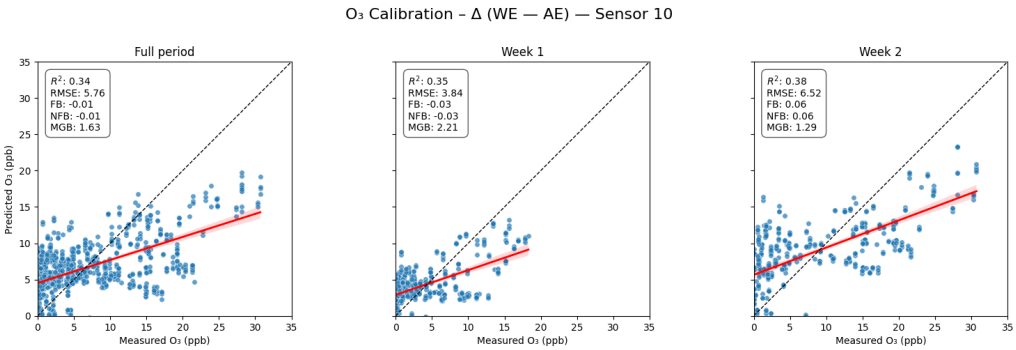

Figure C.10: Calibration plot - PoliTO10

Acknowledgments

Ringrazio di cuore la mia relatrice, la Prof.ssa Clerico, per avermi motivata a cercare un tema davvero stimolante e per avermi guidata alla scoperta di nuove applicazioni di quanto appreso durante questa magistrale. Un sentito ringraziamento va anche ai dottorandi Davide e Nicole, che mi hanno aiutata in questo lavoro con pazienza e riservandomi molta disponibilità. Se questo lavoro è giunto a compimento, è anche merito vostro.